

# DIAGONALIZATION-BASED PRECONDITIONERS AND GENERALIZED CONVERGENCE BOUNDS FOR PARAOPT

ARNE BOUILLON\*<sup>†</sup>, GIOVANNI SAMAEE\*, AND KARL MEERBERGEN\*

**Abstract.** The ParaOpt algorithm was recently introduced as a time-parallel solver for optimal-control problems with a terminal-cost objective, and convergence results have been presented for the linear diffusive case with implicit-Euler time integrators. We reformulate ParaOpt for tracking problems and provide generalized convergence analyses for both objectives. We focus on linear diffusive equations and prove convergence bounds that are generic in the time integrators used. For large problem dimensions, ParaOpt’s performance depends crucially on having a good preconditioner to solve the arising linear systems. For the case where ParaOpt’s cheap, coarse-grained propagator is linear, we introduce diagonalization-based preconditioners inspired by recent advances in the Para-Diag family of methods. These preconditioners not only lead to a weakly-scalable ParaOpt version, but are themselves invertible in parallel, making maximal use of available concurrency. They have proven convergence properties in the linear diffusive case that are generic in the time discretization used, similarly to our ParaOpt results. Numerical results confirm that the iteration count of the iterative solvers used for ParaOpt’s linear systems becomes constant in the limit of an increasing processor count. The paper is accompanied by a sequential MATLAB implementation.

**Key words.** Optimal control, ParaOpt algorithm, preconditioning, parallel-in-time

**MSC codes.** 49M05, 65F08, 65K10, 65Y05

**1. Introduction.** We study algorithms to solve the optimal-control problem

$$(1.1) \quad \min_{\mathbf{y}, \mathbf{u}} J(\mathbf{y}, \mathbf{u}) \quad \text{such that} \quad \mathbf{y}'(t) = \mathbf{g}(\mathbf{y}(t)) + \mathbf{u}(t) \quad \text{and} \quad \mathbf{y}(0) = \mathbf{y}_{\text{init}}.$$

This problem features a state variable  $\mathbf{y} \in \mathbb{R}^M$  evolving over the time interval  $t \in [0, T]$  with initial value  $\mathbf{y}_{\text{init}}$ , an additive control term  $\mathbf{u} \in \mathbb{R}^M$  and an ODE that determines how  $\mathbf{y}$  evolves under  $\mathbf{u}$ ’s influence, including a potentially non-linear function  $\mathbf{g}$ . Bold-faced variables denote vectors. We call  $J$  the *objective function*, as we want to choose  $\mathbf{u}$  to minimize  $J$ . We are interested in *tracking* and *terminal-cost* objectives

$$(1.2) \quad J(\mathbf{y}, \mathbf{u}) = \begin{cases} \text{Tracking:} & \frac{1}{2} \int_0^T \|\mathbf{y}(t) - \mathbf{y}_d(t)\|_2^2 dt + \frac{\gamma}{2} \int_0^T \|\mathbf{u}(t)\|_2^2 dt, \\ \text{Terminal cost:} & \frac{1}{2} \|\mathbf{y}(T) - \mathbf{y}_{\text{target}}\|_2^2 + \frac{\gamma}{2} \int_0^T \|\mathbf{u}(t)\|_2^2 dt. \end{cases}$$

Both use a regularization parameter  $\gamma > 0$  that penalizes large control actions.

As can be found in, for example, [5, 24, 11], a minimum of the optimal-control problem (1.1) must satisfy the *optimality system*

$$(1.3a) \quad \mathbf{y}'(t) = \mathbf{g}(\mathbf{y}(t)) - \boldsymbol{\lambda}(t)/\gamma, \quad \mathbf{y}(0) = \mathbf{y}_{\text{init}}$$

$$(1.3b) \quad \begin{cases} \text{Tracking:} & \boldsymbol{\lambda}'(t) = -\mathbf{g}'(\mathbf{y}(t)) * \boldsymbol{\lambda}(t) + \mathbf{y}_d(t) - \mathbf{y}(t), \quad \boldsymbol{\lambda}(T) = \mathbf{0}, \\ \text{Terminal cost:} & \boldsymbol{\lambda}'(t) = -\mathbf{g}'(\mathbf{y}(t)) * \boldsymbol{\lambda}(t), \quad \boldsymbol{\lambda}(T) = \mathbf{y}(T) - \mathbf{y}_{\text{target}}, \end{cases}$$

which corresponds to solving a boundary value problem (BVP) in the state variable  $\mathbf{y}(t)$  and the *adjoint* variable  $\boldsymbol{\lambda}(t) := -\gamma \mathbf{u}(t)$ . We currently place no restrictions on the function  $\mathbf{g}$ , but from section 3 onward, our analyses and preconditioners will require a linear  $\mathbf{g}(\mathbf{y}(t)) = -K\mathbf{y}(t)$  where  $K \in \mathbb{R}^{M \times M}$ .

\*NUMA, Department of Computer Science, KU Leuven, Leuven, Belgium

<sup>†</sup>Corresponding author: arne.bouillon@kuleuven.be

	$\hat{\lambda}$	$\hat{L}$	$\hat{\sigma}$	$\hat{\gamma}$
Tracking	$\lambda/\sqrt{\gamma}$	$L-1$	$\Delta T\sigma$	$\Delta T/\sqrt{\gamma}$
Terminal cost	$\lambda$	$L$	$\Delta T\sigma$	$\Delta T/\gamma$

Table 2.1: Definitions of  $\hat{\lambda}$ ,  $\hat{L}$ ,  $\hat{\sigma}$  and  $\hat{\gamma}$  for each objective function

To make optimal use of increasingly parallel hardware, a lot of attention has recently been drawn to *time-parallel* methods for solving initial-value problems (IVPs). Many time-parallel approaches to optimal control incorporate IVP solvers as subroutines in an optimization loop [9, 21]. This is a very general approach; however, the speed-up can be limited [5]. Optimal-control problems such as (1.1)–(1.2) can be solved directly with the BVP (1.3). The time-parallel ParaDiag algorithm for IVPs [16, 7, 6], for example, has been extended to these optimality systems for wave equations [23] and parabolic equations [24]. The BVP approach is well-suited to *multiple shooting* (subdividing the time interval), which can enable faster convergence [5, 18].

The Parareal IVP solver [12] has a BVP equivalent in ParaOpt [5], which is the main subject of this paper. Reviewed in section 2, the ParaOpt method decomposes the time interval into sub-intervals – on which parallel solvers are deployed – and ensures that the state and adjoint state on interval boundaries match through an inexact-Newton procedure. ParaOpt was formulated for terminal-cost objectives, with convergence results for linear diffusive problems, in [5]. This paper extends ParaOpt to the tracking optimality system. For both objectives in (1.2), we prove bounds on ParaOpt’s convergence – for linear diffusive equations – that are generic in the time integrators used. This stands in contrast to the existing terminal-cost bound, which specifically holds for implicit Euler. Section 3 contains these convergence results, although some proofs are postponed to sections 5 and 6 for ease of presentation. We then introduce diagonalization-based preconditioners for ParaOpt in section 4. Our bounds and the performance of our preconditioners are confirmed by numerical tests in section 7, after which section 8 concludes the paper.

**2. The ParaOpt algorithm.** The ParaOpt algorithm [5] for time-parallel optimal control was formulated for terminal-cost objectives. We review this method, but use a slightly more general formulation that also allows for the tracking objective.

*Remark 2.1* (Rescaling and circumflexes). For tracking, define  $\hat{\lambda} := \lambda/\sqrt{\gamma}$ ; this rescaling introduces symmetry between the forward and backward equations of the BVP (1.3) and the subproblem of finding  $\hat{\lambda}$  is generally easier (see also [23, 24]).

There will be many similarities between the tracking and terminal-cost cases throughout the paper. To highlight this and simplify notation, we use variables with a  $\hat{\cdot}$  diacritic whose definition depends on the objective, summarized in Table 2.1. For example, terminal cost uses  $\hat{\lambda} := \lambda$ . The other variables are defined in due course.

To solve the optimality system (1.3), ParaOpt starts by dividing  $[0, T]$  into  $L$  sub-intervals  $\{[T_{l-1}, T_l]\}_{l=1}^L$ . We will assume these to be equally large:  $T_l - T_{l-1} = \Delta T$  for all  $l$ . We then introduce approximations  $\{\mathbf{y}_l\}_{l=1}^L$  and  $\{\hat{\lambda}_l\}_{l=1}^L$  to  $\mathbf{y}(t = l\Delta T)$  and  $\hat{\lambda}(t = l\Delta T)$ . Here, the range 1 to  $\hat{L}$  (see Table 2.1) is justified by boundary values either being given as boundary conditions, or not being needed to compute the other unknowns. We define *propagators*  $\mathcal{P}$  and  $\mathcal{Q}$  that approximately solve the BVP (1.3) on the smaller interval  $[T_{l-1}, T_l]$  and with the altered boundary conditions  $\mathbf{y}(T_{l-1}) = \mathbf{y}_{l-1}$  and  $\hat{\lambda}(T_l) = \hat{\lambda}_l$ . Specifically, we have

$$(2.1) \quad \mathcal{P}(T_{l-1}, T_l, \mathbf{y}_{l-1}, \hat{\lambda}_l) \approx \mathbf{y}_l \quad \text{and} \quad \mathcal{Q}(T_{l-1}, T_l, \mathbf{y}_{l-1}, \hat{\lambda}_l) \approx \hat{\lambda}_{l-1} \quad \text{for all } l,$$

such that  $\mathcal{P}$  and  $\mathcal{Q}$  propagate the state forward and adjoint state backward, respectively, over the sub-interval  $[T_{l-1}, T_l]$ . For notational conciseness, we will omit the first two arguments from  $\mathcal{P}$  and  $\mathcal{Q}$  when they are clear from context. The system (1.3) can be solved by composing  $\mathcal{P}$  and  $\mathcal{Q}$  over the sub-intervals if the boundary values are correct, and if the state and adjoint variables are continuous at interval boundaries. These are called the *matching conditions*. Define the concatenations  $\mathbf{y} = [\mathbf{y}_1^\top, \dots, \mathbf{y}_{\hat{L}}^\top]^\top$  and  $\hat{\boldsymbol{\lambda}} = [\hat{\boldsymbol{\lambda}}_1^\top, \dots, \hat{\boldsymbol{\lambda}}_{\hat{L}}^\top]^\top$ , and the variable

$$(2.2) \quad \hat{Q} = \begin{cases} \text{Tracking:} & \mathbf{y}_{\hat{L}} - \mathbf{y}_{\text{target}}, \\ \text{Terminal cost:} & \mathcal{Q}(\mathbf{y}_{\hat{L}}, \mathbf{0}). \end{cases}$$

Then the matching conditions can be written as the non-linear system

$$(2.3) \quad \mathbf{f} \left( \begin{bmatrix} \mathbf{y} \\ \hat{\boldsymbol{\lambda}} \end{bmatrix} \right) := \begin{bmatrix} \mathbf{y}_1 - \mathcal{P}(\mathbf{y}_{\text{init}}, \boldsymbol{\lambda}_1) \\ \vdots \\ \mathbf{y}_{\hat{L}-1} - \mathcal{P}(\mathbf{y}_{\hat{L}-2}, \boldsymbol{\lambda}_{\hat{L}-1}) \\ \mathbf{y}_{\hat{L}} - \mathcal{P}(\mathbf{y}_{\hat{L}-1}, \boldsymbol{\lambda}_{\hat{L}}) \\ \hat{\boldsymbol{\lambda}}_1 - \mathcal{Q}(\mathbf{y}_1, \hat{\boldsymbol{\lambda}}_2) \\ \vdots \\ \hat{\boldsymbol{\lambda}}_{\hat{L}-1} - \mathcal{Q}(\mathbf{y}_{\hat{L}-1}, \hat{\boldsymbol{\lambda}}_{\hat{L}}) \\ \hat{\boldsymbol{\lambda}}_{\hat{L}} - \hat{Q} \end{bmatrix} = \mathbf{0},$$

which can be solved with Newton's method (introducing iteration index  $k$ )

$$(2.4) \quad \mathbf{f}' \left( \begin{bmatrix} \mathbf{y}^{k-1} \\ \hat{\boldsymbol{\lambda}}^{k-1} \end{bmatrix} \right) \begin{bmatrix} \mathbf{y}^k - \mathbf{y}^{k-1} \\ \hat{\boldsymbol{\lambda}}^k - \hat{\boldsymbol{\lambda}}^{k-1} \end{bmatrix} = -\mathbf{f} \left( \begin{bmatrix} \mathbf{y}^{k-1} \\ \hat{\boldsymbol{\lambda}}^{k-1} \end{bmatrix} \right)$$

where the Jacobian  $\mathbf{f}' \left( \begin{bmatrix} \mathbf{y} \\ \hat{\boldsymbol{\lambda}} \end{bmatrix} \right) =$

$$(2.5) \quad \begin{bmatrix} \begin{array}{ccc|ccc} I & & & -\mathcal{P}_\lambda(\mathbf{y}_{\text{init}}, \hat{\boldsymbol{\lambda}}_1) & & \\ -\mathcal{P}_y(\mathbf{y}_1, \hat{\boldsymbol{\lambda}}_2) & I & & & -\mathcal{P}_\lambda(\mathbf{y}_1, \hat{\boldsymbol{\lambda}}_2) & \\ & \ddots & & & \ddots & \\ & & -\mathcal{P}_y(\mathbf{y}_{L-1}, \hat{\boldsymbol{\lambda}}_L) & I & & -\mathcal{P}_\lambda(\mathbf{y}_{L-1}, \hat{\boldsymbol{\lambda}}_L) \\ \hline -\mathcal{Q}_y(\mathbf{y}_1, \hat{\boldsymbol{\lambda}}_2) & & & I & -\mathcal{Q}_\lambda(\mathbf{y}_1, \hat{\boldsymbol{\lambda}}_2) & \\ & \ddots & & & \ddots & \\ & & -\mathcal{Q}_y(\mathbf{y}_{L-1}, \hat{\boldsymbol{\lambda}}_L) & & I & -\mathcal{Q}_\lambda(\mathbf{y}_{L-1}, \hat{\boldsymbol{\lambda}}_L) \\ & & & & & I \\ & & & & & -\frac{\partial \hat{Q}}{\partial \mathbf{y}_{\hat{L}}} \end{array} \end{bmatrix}$$

with  $\cdot_y := \frac{\partial}{\partial \mathbf{y}}$  and  $\cdot_\lambda := \frac{\partial}{\partial \boldsymbol{\lambda}}$ . These derivative terms are expensive to compute; this sparks interest in an *inexact Newton iteration*, which only requires an approximate Jacobian. To this end, the authors in [5] replace  $\mathcal{P}_y$ ,  $\mathcal{P}_\lambda$ ,  $\mathcal{Q}_y$ , and  $\mathcal{Q}_\lambda$  by derivatives of coarse, approximate propagators  $\tilde{\mathcal{P}}$  and  $\tilde{\mathcal{Q}}$ . This results in an approximate Jacobian

$$(2.6) \quad \tilde{\mathbf{f}}' \approx \mathbf{f}'.$$

The ParaOpt algorithm, then, is to approximate (2.4) – in each iteration of the Newton procedure – by using an inner iterative solver such as GMRES that uses the coarse propagators  $\tilde{\mathcal{P}}$  and  $\tilde{\mathcal{Q}}$  to evaluate multiplications by an approximate Jacobian  $\tilde{\mathbf{f}}'$ . Such multiplication is embarrassingly parallelizable, since each element in the resulting vector can be calculated independently.





We can now give some values of  $\varphi$  and  $\psi$  for various propagators and objectives.

LEMMA 3.5. *For tracking objectives, (FOTD) implicit Euler with  $J$  length- $\tau$  steps (i.e.,  $\Delta T = J\tau$ ) applied to a linear diffusive problem satisfies Assumptions 3.1 to 3.3 with*

$$(3.11) \quad \varphi = \varphi_\tau^{(J)} \quad \text{and} \quad \psi = \psi_\tau^{(J)}$$

where  $\varphi_\tau^{(0)} = 1$  and  $\psi_\tau^{(0)} = 0$  and, with  $\zeta := (1 + \sigma_\tau)$ , we have the recursion

$$(3.12) \quad \varphi_\tau^{(j+1)} = \varphi_\tau^{(j)}(\zeta^{-1} - \widehat{\gamma}_\tau(\psi_\tau^{(j+1)} - \widehat{\gamma}_\tau\zeta^{-1})) \quad \text{and} \quad \psi_\tau^{(j+1)} = \frac{\widehat{\gamma}_\tau + \zeta^{-1}(1 + \widehat{\gamma}_\tau^2)\psi_\tau^{(j)}}{\zeta + \widehat{\gamma}_\tau\psi_\tau^{(j)}}.$$

*Proof.* This result is derived in Appendix A.2.  $\square$

LEMMA 3.6. *For tracking objectives, exact solvers on a linear diffusive problem satisfy Assumptions 3.1 to 3.3 with*

$$(3.13) \quad \varphi = d^{-1} \quad \text{and} \quad \psi = -d^{-1}c,$$

where  $c = -\widehat{\gamma} \frac{\sinh(\sqrt{\widehat{\gamma}^2 + \widehat{\sigma}^2})}{\sqrt{\widehat{\gamma}^2 + \widehat{\sigma}^2}}$  and  $d = \cosh(\sqrt{\widehat{\gamma}^2 + \widehat{\sigma}^2}) + \widehat{\sigma} \frac{\sinh(\sqrt{\widehat{\gamma}^2 + \widehat{\sigma}^2})}{\sqrt{\widehat{\gamma}^2 + \widehat{\sigma}^2}}.$

*Proof.* This result is derived in Appendix A.3.  $\square$

LEMMA 3.7. *For terminal cost, FDTO implicit Euler with  $J$  length- $\tau$  steps (i.e.,  $\Delta T = J\tau$ ) applied to a linear diffusive problem satisfies Assumptions 3.1 to 3.3 with*

$$(3.14) \quad \varphi = (1 + \sigma\tau)^{-J} \quad \text{and} \quad \psi = \frac{1 - \varphi^2}{\gamma\sigma(2 + \sigma\tau)}.$$

*Proof.* This result is found in [5, (3.16)–(3.17)].  $\square$

LEMMA 3.8. *For terminal cost, FOTD implicit Euler with  $J$  length- $\tau$  steps (i.e.,  $\Delta T = J\tau$ ) applied to a linear diffusive problem satisfies Assumptions 3.1 to 3.3 with*

$$(3.15) \quad \varphi = (1 + \sigma\tau)^{-J} \quad \text{and} \quad \psi = \frac{(1 - \varphi_\tau^2)(1 + \widehat{\sigma}_\tau)}{\gamma\sigma(2 + \sigma\tau)}.$$

*Proof.* This result can be derived analogously to Lemma 3.5.  $\square$

LEMMA 3.9. *For terminal cost, exact solvers on a linear diffusive problem satisfy Assumptions 3.1 to 3.3 with*

$$(3.16) \quad \varphi = d^{-1} \quad \text{and} \quad \psi = -d^{-1}b, \quad \text{where} \quad b = -\widehat{\gamma} \frac{\sinh \widehat{\sigma}}{\widehat{\sigma}} \quad \text{and} \quad d = \exp \widehat{\sigma}.$$

*Proof.* This result can be derived analogously to Lemma 3.6.  $\square$

**3.2. Convergence results.** Terminal-cost ParaOpt was proposed in [5], which includes a convergence bound for the case where both the fine and the coarse propagators use FDTO implicit Euler. We propose alternative bounds  $\rho^*$  on ParaOpt's convergence factor  $\rho$  that are generic in the propagators used. Theorems 3.10 and 3.12 treat tracking and terminal cost, respectively.

THEOREM 3.10. *When tracking ParaOpt is applied to a linear diffusive equation and Assumptions 3.1 to 3.3 hold, the convergence factor  $\rho$  satisfies*

$$(3.17) \quad \rho < \rho^* := \max_{\sigma \in \text{eig}(K)} \sqrt{\frac{(\tilde{\varphi} - \varphi)^2 + (\tilde{\psi} - \psi)^2}{(1 - \tilde{\varphi})^2 + \tilde{\psi}^2}}.$$

*Proof.* Section 5 is dedicated to proving this result.  $\square$

The  $\varphi$ ,  $\psi$ ,  $\tilde{\varphi}$ , and  $\tilde{\psi}$  values for a specific set of propagators can be filled in to the general bound given in Theorem 3.10. We give an example.

*Example 3.11.* Consider tracking ParaOpt applied to a linear diffusive equation with an exact fine propagator and a one-step implicit-Euler coarse one. Then we can combine the results from Lemmas 3.5 and 3.6 with (3.17) to bound  $\rho$ . In fact, in this specific case, we can prove that

$$(3.18) \quad \rho < \rho^* < 1$$

for any  $\sigma$ ,  $\gamma$ , and  $\Delta T$ , meaning that ParaOpt does not diverge. The bound (3.18) is proven in Appendix A.4.

**THEOREM 3.12.** *When terminal-cost ParaOpt is applied to a linear diffusive equation and Assumptions 3.1 to 3.3 hold, the convergence factor  $\rho$  satisfies*

$$(3.19) \quad \rho \leq \rho^* := \max_{\sigma \in \text{eig}(K)} \max \left( \frac{|\varphi - \tilde{\varphi}|}{1 - \tilde{\varphi}}, x^* \right),$$

where  $x^*$  is the root of  $f_\infty(x) := \frac{\tilde{\psi} - \psi}{\tilde{\psi} + 1 / \sum_{l=0}^{\infty} (\tilde{\varphi} + \frac{\varphi - \tilde{\varphi}}{x})^{2l}} - x$  with the largest magnitude.

*Proof.* Section 6 is dedicated to proving this result.  $\square$

Note that, while its definition is implicit,  $x^*$  in Theorem 3.12 is efficiently computable. This is elaborated upon at the end of section 6.

**3.3. Interpreting the convergence results.** The  $\rho$  bounds (3.17) and (3.19) are generic in the propagators used (under Assumptions 3.1 to 3.3) and independent of  $\hat{L}$ . The latter property not only results in efficiently computable bounds (as opposed to calculating eigenvalues of potentially large matrices), but also ensures that the number of ParaOpt iterations stays constant when increasing  $T$  together with  $\hat{L}$ . We return to this scaling in subsection 4.1.

To investigate specific propagators, their  $\varphi$  and  $\psi$  can be calculated as a function of the problem parameters  $\sigma$ ,  $\gamma$ , and  $\tau$ . Appendix A.1 goes into more detail about this procedure. A bound on  $\rho$  can then be obtained by filling  $\varphi$  and  $\psi$  into (3.17) and (3.19). Let us do so for an exact fine propagator (or, equivalently, a numerical propagator in the limit for infinitely small time steps) and an implicit-Euler coarse propagator. Recall from Remark 3.4 that, in the case of terminal cost, two implicit-Euler discretizations are possible: either first-discretize-then-optimize (as [5] uses) or the other way around. We will compare both techniques.

Figure 3.1 shows  $\rho^*$  as a function of the problem parameters  $\hat{\sigma}$  and  $\hat{\gamma}$ . Recall that  $\rho^*$  is an upper bound on ParaOpt's convergence factor;  $\rho^* < 1$  means guaranteed convergence and, as  $\rho^*$  decreases further, this convergence accelerates. In the tracking case, Figure 3.1a confirms the result (3.18), which guarantees  $\rho$  never exceeds 1. For terminal cost, Figures 3.1c and 3.1d show the bound (3.19) for FOTD implicit Euler; Figures 3.1e and 3.1f concern FDTO. With an exact fine propagator, it is clear that our FOTD coarse propagators never cause divergence for linear diffusive problems, while those based on FDTO might. Figure 3.2 shows the ratio of the bounds  $\rho^*$  from Figures 3.1c and 3.1e, comparing the FOTD and FDTO strategies. This analysis showcases the advantage of having generic results: we can study these two propagators side-by-side, while previous bounds were specific to a single propagator choice. To assess the quality of our upper bound, we compare it to the one given by [5, Corollary 3.6 and Theorem 3.8] in Figure 3.3. This shows the novel bound to be at least as tight as the existing one.

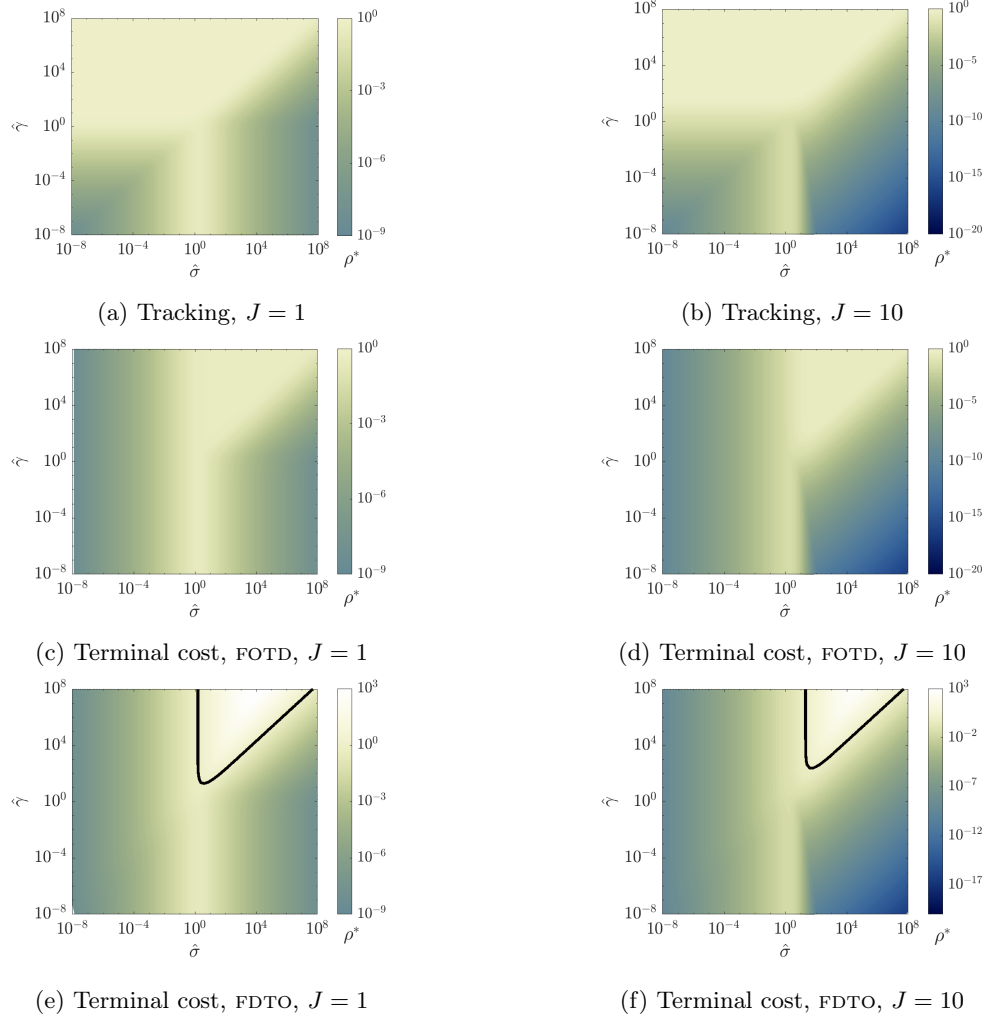


Fig. 3.1: The bound (3.17) or (3.19) on ParaOpt's convergence factor  $\rho^*$  is shown, with an exact fine and a  $J$ -step implicit-Euler coarse propagator. Recall that  $\rho^* < 1$  guarantees convergence. The black contour lines mark  $\rho^* = 1$ .

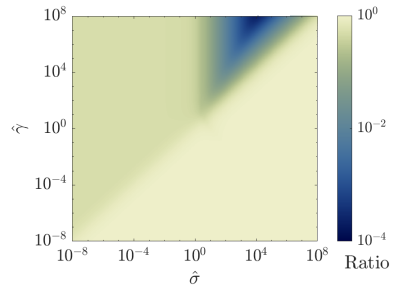


Fig. 3.2: Ratio of the  $\rho^*$  values in Figures 3.1c and 3.1e

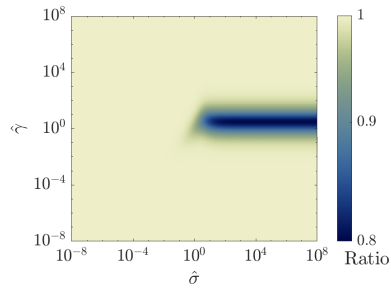


Fig. 3.3: Ratio of  $\rho^*$  in Figure 3.1e with that of the bound in [5]



**4. Diagonalization-based preconditioners.** Having presented the ParaOpt algorithm and studied its convergence, we will now consider its scaling in subsection 4.1, establishing the need for efficient preconditioners in the inexact-Newton step. For affine coarse propagators, we propose in subsections 4.2 and 4.3 to construct a preconditioner that uses *alpha-circulant* approximations of the system matrix, which can be inverted efficiently by a diagonalization procedure. Subsection 4.4 then details how to solve the arising smaller linear systems, after which subsection 4.5 mentions some properties of the preconditioners that influence the convergence of iterative solvers.

**4.1. Scaling ParaOpt and the need for preconditioners.** When ParaOpt uses time integrators that satisfy Assumptions 3.1 to 3.3,  $\rho^*$  in Theorems 3.10 and 3.12 is an upper bound on the rate of the algorithm's exponential convergence. When the number of intervals  $L$  is increased – which scales both the problem size and the available parallelism – we study the evolution of  $\rho^*$  in two regimes of *weak scaling* [5].

- When  $T$  and  $L$  are increased together,  $\hat{\sigma}$  and  $\hat{\gamma}$  do not change. Given that our bounds are  $L$ -independent,  $\rho^*$  stays constant and the upper bound on the number of ParaOpt iterations is independent of the available parallelism.
- When  $T$  is kept constant,  $\Delta T$  – and with it,  $\hat{\sigma}$  and  $\hat{\gamma}$  – decreases instead. Scaling  $L$  then corresponds to traversing the graphs in Figure 3.1 in a diagonal line towards the region with small  $\hat{\sigma}$  and  $\hat{\gamma}$ . In, [5], it already noted that  $\rho^*$  is bounded in this scaling regime for FDTO implicit-Euler propagators on a linear diffusive terminal-cost problem. Our graphs allow similar conclusions and can be drawn for any propagators satisfying Assumptions 3.1 to 3.3. In Figure 3.1's examples,  $\rho^*$  even goes to zero in the scaling limit, surpassing the usual concept of weak scalability. In the non-asymptotic regime, weak scalability may be absent until the maximum at  $\hat{\sigma} \approx 1$  has been surmounted.

It follows from this discussion that, if the amount of work in each ParaOpt iteration scales linearly with  $L$ , the algorithm is weakly scalable for linear diffusive problems (and, experimentally, more broadly [5]). This condition, however, is not yet fulfilled. The inexact-Newton procedure solves, in each iteration, a linear system with a matrix of size  $(2M\hat{L} \times 2M\hat{L})$ . With a direct or non-preconditioned iterative method, the cost of this scales superlinearly with  $\hat{L}$  (and thus with  $L$ ), which – especially if  $K \in \mathbb{R}^{M \times M}$  is large but sparse – starts to dominate the algorithm's execution time.

Hence our mission in the rest of this section is to precondition these systems such that the cost of solving them with iterative methods is linear in  $L$ . Each iteration of the iterative solver uses a matrix multiplication and an inversion, which will both scale (log-)linearly with  $L$ . The number of iterations should then be constant.

**4.2. Linear coarse-grid correction.** Our preconditioners will apply to affine coarse propagators (that is,  $\tilde{\mathcal{P}}$  and  $\tilde{\mathcal{Q}}$  are of the forms (3.1c) and (3.1d)). Then the inexact-Newton step – *coarse-grid correction*, in Parareal vernacular – looks like

$$(4.1) \quad \tilde{A} \begin{bmatrix} \mathbf{y}^k - \mathbf{y}^{k-1} \\ \hat{\lambda}^k - \hat{\lambda}^{k-1} \end{bmatrix} = -\mathbf{f} \left( \begin{bmatrix} \mathbf{y}^{k-1} \\ \hat{\lambda}^{k-1} \end{bmatrix} \right)$$

where the matrix  $\tilde{A}$  can be written as (using  $\otimes$  to denote a Kronecker product)

$$(4.2) \quad \tilde{A} = \begin{bmatrix} I \otimes I + B \otimes \tilde{\Phi}_{\mathcal{P}} & I \otimes \tilde{\Psi}_{\mathcal{P}} \\ -I \otimes \tilde{\Psi}_{\mathcal{Q}} + E \otimes (\tilde{\Psi}_{\mathcal{Q}} - \partial \hat{\mathcal{Q}} / \partial \mathbf{y}_{\hat{L}}) & I \otimes I + B^{\top} \otimes \tilde{\Phi}_{\mathcal{Q}} \end{bmatrix}.$$

Here,  $\hat{\mathcal{Q}}$  is as defined in (2.2),  $E$  is a matrix with as only non-zero a one in its bottom-right corner, and  $B$  only has  $(-1)$ s on its first sub-diagonal.

**4.3. Formulating the preconditioners.** Inspired by work on parallelizing the coarse-grid correction of Parareal [22], we propose a low-rank perturbation of  $\tilde{A}$  in (4.2) as a preconditioner. Introduce a parameter  $\alpha \in \mathbb{C}$  and define

$$(4.3) \quad P(\alpha) := \begin{bmatrix} I \otimes I + C(\alpha) \otimes \tilde{\Phi}_{\mathcal{P}} & I \otimes \tilde{\Psi}_{\mathcal{P}} \\ -I \otimes \tilde{\Psi}_{\mathcal{Q}} & I \otimes I + C^*(\alpha) \otimes \tilde{\Phi}_{\mathcal{Q}} \end{bmatrix},$$

where  $C(\alpha)$  differs from  $B$  only by an additional non-zero value of  $-\alpha$  in the top-right corner. This preconditioner contains two modifications compared to  $\tilde{A}$ :

- Replacing  $B$  by  $C(\alpha)$  causes a rank- $(2M)$  perturbation, which is scaled by  $\alpha$ .
- The term  $E \otimes (\tilde{\Psi}_{\mathcal{Q}} - \partial\hat{Q}/\partial\mathbf{y}_{\hat{L}})$  has been left out. This has no effect in the tracking case, but is a rank- $M$  perturbation for terminal cost (although it combines with the perturbation above to another rank- $(2M)$  perturbation).

The preconditioner is itself invertible by a parallel process, as will be explained next. We outline two methods to perform this inversion: a general one, which requires us to choose  $|\alpha| = 1$ , and one for the case  $\tilde{\Psi}_{\mathcal{Q}} = O$ , which can use any  $\alpha \neq 0$ .

*General method.* The matrix  $C(\alpha)$  used in (4.3) is an *alpha-circulant* matrix – that is, it is Toeplitz and each super-diagonal is equal to a value  $\alpha$  times its complementing sub-diagonal. It is well-known (see, e.g., [1]) that alpha-circulants diagonalize as

$$(4.4) \quad C(\alpha) = VD(\alpha)V^{-1} \quad \text{with} \quad V = \Gamma_{\alpha}^{-1}\mathbb{F}^* \quad \text{and} \quad D(\alpha) = \text{diag}(\sqrt{\hat{L}}\mathbb{F}\Gamma_{\alpha}\mathbf{e}_1(\alpha))$$

where  $\mathbf{e}_1(\alpha)$  is  $C(\alpha)$ 's first column,  $\mathbb{F} = \{e^{2\pi ijk/\hat{L}}/\sqrt{\hat{L}}\}_{j,k=0}^{\hat{L}-1}$  is the discrete Fourier matrix, and we define  $\Gamma_{\alpha} = \text{diag}(1, \alpha^{1/\hat{L}}, \dots, \alpha^{(\hat{L}-1)/\hat{L}})$ . When  $|\alpha| = 1$ , it holds that  $\Gamma_{\alpha}^{-1} = \Gamma_{\alpha}^*$  (where  $\Gamma_{\alpha}^*$  is the Hermitian transpose of  $\Gamma_{\alpha}$ ) and, therefore,  $C(\alpha)$  and  $C^*(\alpha)$  are simultaneously diagonalizable [2]. Then

$$P^{-1}(\alpha) = \left( \begin{bmatrix} \Gamma_{\alpha}^*\mathbb{F}^* & \\ & \Gamma_{\alpha}^*\mathbb{F}^* \end{bmatrix} \otimes I \right) \begin{bmatrix} I \otimes I + D(\alpha) \otimes \tilde{\Phi}_{\mathcal{P}} & I \otimes \tilde{\Psi}_{\mathcal{P}} \\ -I \otimes \tilde{\Psi}_{\mathcal{Q}} & I \otimes I + D^*(\alpha) \otimes \tilde{\Phi}_{\mathcal{Q}} \end{bmatrix}^{-1} \left( \begin{bmatrix} \mathbb{F}\Gamma_{\alpha} & \\ & \mathbb{F}\Gamma_{\alpha} \end{bmatrix} \otimes I \right),$$

where the inverted matrix on the right-hand side has only diagonal matrices as left operands in the Kronecker products. Thus inversion of  $P(\alpha)$  can be decomposed into  $\hat{L}$  different inversions that can be solved in parallel, as implemented in Algorithm 4.1. The Fourier matrix  $\mathbb{F}$  can be applied efficiently (log-linearly in  $L$ ) with the fast Fourier transform and can be parallelized over the spatial dimensions of the problem.

---

**Algorithm 4.1** Procedure for inverting  $P(\alpha)$  from (4.3)

---

**Input:** Vectors  $\mathbf{v}$  and  $\mathbf{w}$

Matrix  $D(\alpha)$  following from the time discretization by (4.4) ( $|\alpha| = 1$ ) with diagonal elements  $d_l(\alpha)$

**Output:** The vector  $\begin{bmatrix} \mathbf{x} \\ \mathbf{z} \end{bmatrix} = P^{-1}(\alpha) \begin{bmatrix} \mathbf{v} \\ \mathbf{w} \end{bmatrix}$

- 1: Calculate  $\mathbf{r}_1 := (\mathbb{F}\Gamma_{\alpha} \otimes I)\mathbf{v}$ ,  $\mathbf{s}_1 := (\mathbb{F}\Gamma_{\alpha} \otimes I)\mathbf{w}$  using the (parallel) FFT.
- 2: For  $l = \{1, \dots, \hat{L}\}$ , solve (in parallel)

$$(4.5) \quad \begin{bmatrix} \mathbf{r}_{2,l} \\ \mathbf{s}_{2,l} \end{bmatrix} := \begin{bmatrix} I + d_l(\alpha)\tilde{\Phi}_{\mathcal{P}} & \tilde{\Psi}_{\mathcal{P}} \\ -\tilde{\Psi}_{\mathcal{Q}} & I + d_l^*(\alpha)\tilde{\Phi}_{\mathcal{Q}} \end{bmatrix}^{-1} \begin{bmatrix} \mathbf{r}_{1,l} \\ \mathbf{s}_{1,l} \end{bmatrix}.$$

- 3: Calculate  $\mathbf{x} = (\Gamma_{\alpha}^{-1}\mathbb{F}^* \otimes I)\mathbf{r}_2$ ,  $\mathbf{z} = (\Gamma_{\alpha}^{-1}\mathbb{F}^* \otimes I)\mathbf{s}_2$  using the (parallel) FFT.
-

*Method for a block-triangular preconditioner.* When  $\tilde{\Psi}_{\mathcal{Q}} = O$  (as is often the case for terminal-cost objectives), we can invert the bottom and top halves of  $P(\alpha)$  separately. Then simultaneous diagonalizability of  $C(\alpha)$  and  $C^*(\alpha)$  is no longer needed and  $\alpha$  can be any non-zero number (with small values generally working better [2], as they decrease the difference between  $P(\alpha)$  and  $\tilde{A}$ ). Then it holds that

$$P^{-1}(\alpha) = \left( \begin{bmatrix} \Gamma_{\alpha}^{-1} \mathbb{F}^* & \\ & \Gamma_{\alpha}^* \mathbb{F}^* \end{bmatrix} \otimes I \right) \left[ \begin{array}{c} I \otimes I + D(\alpha) \otimes \tilde{\Phi}_{\mathcal{P}} \quad (\mathbb{F}\Gamma_{\alpha} \Gamma_{\alpha}^* \mathbb{F}^*) \otimes \tilde{\Psi}_{\mathcal{P}} \\ I \otimes I + D^*(\alpha) \otimes \tilde{\Phi}_{\mathcal{Q}} \end{array} \right]^{-1} \left( \begin{bmatrix} \mathbb{F}\Gamma_{\alpha} & \\ & \mathbb{F}\Gamma_{\alpha}^{-*} \end{bmatrix} \otimes I \right).$$

Algorithm 4.2 lays out how to multiply a vector by  $P^{-1}(\alpha)$  when using this method.

---

**Algorithm 4.2** Procedure for inverting  $P(\alpha)$  from (4.3) when  $\tilde{\Psi}_{\mathcal{Q}} = O$

---

**Input:** Vectors  $\mathbf{v}$  and  $\mathbf{w}$

Matrix  $D(\alpha)$  following from the time discretization by (4.4) ( $|\alpha| \neq 0$ ) with diagonal elements  $d_l(\alpha)$

**Output:** The vector  $\begin{bmatrix} \mathbf{x} \\ \mathbf{z} \end{bmatrix} = P^{-1}(\alpha) \begin{bmatrix} \mathbf{v} \\ \mathbf{w} \end{bmatrix}$

▷ Phase 1: invert the bottom-right block

1: Calculate  $((\mathbf{s}_{1,1})^{\top}, \dots, (\mathbf{s}_{1,\hat{L}})^{\top})^{\top} := (\mathbb{F}\Gamma_{\alpha}^{-*} \otimes I)\mathbf{w}$  using the (parallel) FFT.

2: For  $l = \{1, \dots, \hat{L}\}$ , solve (in parallel)

$$(4.6) \quad \mathbf{s}_{2,l} := (I + d_l^*(\alpha)\tilde{\Phi}_{\mathcal{Q}})^{-1} \mathbf{s}_{1,l}$$

and assemble  $\mathbf{s}_2 := ((\mathbf{s}_{2,1})^{\top}, \dots, (\mathbf{s}_{2,\hat{L}})^{\top})^{\top}$ .

3: Calculate  $\mathbf{z} = (\Gamma_{\alpha}^* \mathbb{F}^* \otimes I)\mathbf{s}_2$  using the (parallel) FFT.

▷ Phase 2: invert the rest of the matrix

4: Set  $\mathbf{r}_1 = \mathbf{v} - (I \otimes \tilde{\Psi}_{\mathcal{P}})\mathbf{z}$ .

5: Calculate  $((\mathbf{r}_{2,1})^{\top}, \dots, (\mathbf{r}_{2,\hat{L}})^{\top})^{\top} := (\mathbb{F}\Gamma_{\alpha} \otimes I)\mathbf{r}_1$  using the (parallel) FFT.

6: For  $l = \{1, \dots, \hat{L}\}$ , solve (in parallel)

$$(4.7) \quad \mathbf{r}_{3,l} := (I + d_l(\alpha)\tilde{\Phi}_{\mathcal{P}})^{-1} \mathbf{r}_{2,l}$$

and assemble  $\mathbf{r}_3 := ((\mathbf{r}_{3,1})^{\top}, \dots, (\mathbf{r}_{3,\hat{L}})^{\top})^{\top}$ .

7: Calculate  $\mathbf{x} = (\Gamma_{\alpha}^{-1} \mathbb{F}^* \otimes I)\mathbf{r}_3$  using the (parallel) FFT.

---

**4.4. Solving the smaller systems.** In Algorithms 4.1 and 4.2, it is needed to solve  $\hat{L}$  linear systems in parallel to each other. In the general method (Algorithm 4.1), these systems (4.5) use matrices of the form

$$(4.8) \quad H_l := \begin{bmatrix} I + d_l(\alpha)\tilde{\Phi}_{\mathcal{P}} & \tilde{\Psi}_{\mathcal{P}} \\ -\tilde{\Psi}_{\mathcal{Q}} & I + d_l^*(\alpha)\tilde{\Phi}_{\mathcal{Q}} \end{bmatrix}$$

and this subsection outlines how  $H_l$  can be inverted. This is non-trivial due to the matrices  $\tilde{\Phi}_{\mathcal{P}}$ ,  $\tilde{\Phi}_{\mathcal{Q}}$ ,  $\tilde{\Psi}_{\mathcal{P}}$ , and  $\tilde{\Psi}_{\mathcal{Q}}$ , which are defined through the coarse propagators (3.1c) and (3.1d). We focus on the general method; the specialized case of Algorithm 4.2 is simpler and can be treated analogously. We propose two methods for solving systems with  $H_l$ , differing both in generality and in performance.

*Method 1: Black-box approach.* One strength of the ParaOpt algorithm is that the propagators can be given as black boxes (although for our preconditioners, we do require the coarse ones to be affine). In that case we can only access the  $\tilde{\Phi}$  and  $\tilde{\Psi}$  matrices through the propagators  $\tilde{\mathcal{P}}$  and  $\tilde{\mathcal{Q}}$  by (3.1c) and (3.1d). Without giving up on the black-box character of the coarse solvers, the smaller systems can be tackled with an iterative solver, which only needs  $H_l$  as a multiplication routine. It can be seen that, for any  $\mathbf{x}$  and  $\mathbf{z}$ ,

$$(4.9) \quad H_l \begin{bmatrix} \mathbf{x} \\ \mathbf{z} \end{bmatrix} = \begin{bmatrix} \mathbf{x} + \tilde{\mathcal{P}}(d_l(\alpha)\mathbf{x}, -\mathbf{z}) - \tilde{\mathcal{P}}(\mathbf{0}, \mathbf{0}) \\ \mathbf{z} + \tilde{\mathcal{Q}}(-\mathbf{x}, d_l^*(\alpha)\mathbf{z}) - \tilde{\mathcal{Q}}(\mathbf{0}, \mathbf{0}) \end{bmatrix}$$

where the quantities  $\tilde{\mathcal{P}}(\mathbf{0}, \mathbf{0})$  and  $\tilde{\mathcal{Q}}(\mathbf{0}, \mathbf{0})$  can be precomputed.

*Method 2: Using the coarse propagators' explicit form.* In many cases, the coarse propagators will be simple and their explicit form known. Then it is often possible to solve the linear system more cheaply than with the black-box approach above. Example 4.1 illustrates this for the case of a simple coarse propagator.

*Example 4.1* (Tracking with one-step implicit Euler). ParaOpt with a tracking objective and a one-step implicit-Euler coarse propagator for linear problems has that

$$(4.10) \quad \tilde{\Phi} = (I + \Delta TK)^{-1} \quad \text{and} \quad \tilde{\Psi} = \hat{\gamma}(I + \Delta TK)^{-1},$$

as can be derived using Appendix A.1's arguments. Write  $Z := I + \Delta TK$ . Then

$$(4.11) \quad \begin{bmatrix} I + d_l(\alpha)Z^{-1} & \hat{\gamma}Z^{-1} \\ -\hat{\gamma}Z^{-1} & I + d_l^*(\alpha)Z^{-1} \end{bmatrix} \begin{bmatrix} \mathbf{r}_2 \\ \mathbf{s}_2 \end{bmatrix} = \begin{bmatrix} \mathbf{r}_1 \\ \mathbf{s}_1 \end{bmatrix} \Leftrightarrow \begin{bmatrix} Z + d_l(\alpha)I & \hat{\gamma}I \\ -\hat{\gamma}I & Z + d_l^*(\alpha)I \end{bmatrix} \begin{bmatrix} \mathbf{r}_2 \\ \mathbf{s}_2 \end{bmatrix} = \begin{bmatrix} Z\mathbf{r}_1 \\ Z\mathbf{s}_1 \end{bmatrix}.$$

The second form is much easier to solve, by either direct or iterative methods.

Both approaches above can use iterative solvers, while only method 2 can use direct methods. In the context of IVP ParaDiag algorithms, multiple techniques have been proposed to accelerate solving related linear systems [10, 13]. Adaptations of those methods could conceivably further improve the efficiency of our preconditioner.

**4.5. Convergence results.** To assess the convergence properties of solving systems with  $\tilde{A}$  using the proposed preconditioners  $P(\alpha)$ , we take the usual approach of studying the eigenvalues of the preconditioned system matrix  $P^{-1}(\alpha)\tilde{A}$ . If those are clustered together and lie far enough away from zero, rapid convergence is expected for most iterative linear-system solvers such as GMRES [19].

An advantage of using ParaDiag-inspired preconditioners is that, in certain cases, eigenvalue results from ParaDiag apply directly. In [2], analytic expressions are provided for the preconditioned eigenvalues of optimization ParaDiag methods applied to linear diffusive problems, for both objective functions we study. When Assumptions 3.1 and 3.2 are satisfied *for the coarse propagator*, those eigenvalue expressions also apply to the proposed ParaOpt preconditioners. In particular, for tracking and when choosing  $\alpha = -1$  in (4.3), it is shown in [2] that GMRES converges exponentially with a problem-independent convergence rate under Assumptions 3.1 to 3.3.

Even in the most general situation, where nothing is known about the coarse propagators other than them being affine, preconditioned coarse-grid correction asymptotically scales well with increasing time-parallelism, as the following theorem asserts.

**THEOREM 4.2.** *The preconditioned matrix  $P^{-1}(\alpha)\tilde{A}$  has at most  $2M$  eigenvalues that differ from 1.*

*Proof.* The difference  $\tilde{A} - P(\alpha)$  between the matrices has maximum rank  $2M$ . It is a well-known result (mentioned in, e.g., [23]) that this proves the theorem.  $\square$

**5. Proof of Theorem 3.10.** Given the discussion in subsection 3.1 it holds that  $\rho = \max_{\sigma \in \text{eig}(K)} \max(|\text{eig}(S_\sigma)|)$ , with  $S_\sigma$  given by (3.9a). Define  $B$  and  $\tilde{B}$  such that

$$(5.1) \quad S_\sigma = I - \begin{bmatrix} \tilde{B} & \tilde{\psi}I \\ -\tilde{\psi}I & \tilde{B}^\top \end{bmatrix}^{-1} \begin{bmatrix} B & \psi I \\ -\psi I & B^\top \end{bmatrix}.$$

We will first prove a general result about the eigenvalues  $(1 - \theta)$  of (5.1), making abstraction of the forms of  $B$  and  $\tilde{B}$ .

LEMMA 5.1. *Let  $\theta$  be an eigenvalue of*

$$(5.2) \quad \begin{bmatrix} \tilde{B} & \tilde{\psi}I \\ -\tilde{\psi}I & \tilde{B}^\top \end{bmatrix}^{-1} \begin{bmatrix} B & \psi I \\ -\psi I & B^\top \end{bmatrix}$$

with  $B, \tilde{B} \in \mathbb{R}^{\hat{L} \times \hat{L}}$ . Then, for some vector  $\mathbf{v} \in \mathbb{C}^{\hat{L}}$ ,

$$(5.3) \quad |1 - \theta|^2 = \frac{\mathbf{v}^*((B - \tilde{B})^\top(B - \tilde{B}) + (\psi - \tilde{\psi})^2I)\mathbf{v}}{\mathbf{v}^*(\tilde{B}^\top\tilde{B} + \tilde{\psi}^2I)\mathbf{v}}.$$

*Proof.* The proof of this lemma is inspired by [23], which in turn refers to [20]. An eigenvalue  $\theta$  and its corresponding eigenvector  $(\mathbf{v}^\top, \mathbf{w}^\top)^\top$  satisfy

$$(5.4) \quad \begin{bmatrix} B & \psi I \\ -\psi I & B^\top \end{bmatrix} \begin{bmatrix} \mathbf{v} \\ \mathbf{w} \end{bmatrix} = \theta \begin{bmatrix} \tilde{B} & \tilde{\psi}I \\ -\tilde{\psi}I & \tilde{B}^\top \end{bmatrix} \begin{bmatrix} \mathbf{v} \\ \mathbf{w} \end{bmatrix},$$

which is equivalent to the system

$$(5.5a) \quad B\mathbf{v} + \psi\mathbf{w} = \theta(\tilde{B}\mathbf{v} + \tilde{\psi}\mathbf{w}),$$

$$(5.5b) \quad -\psi\mathbf{v} + B^\top\mathbf{w} = \theta(-\tilde{\psi}\mathbf{v} + \tilde{B}^\top\mathbf{w}).$$

Then from (5.5a) follows

$$(5.6) \quad \mathbf{w} = \frac{\theta\tilde{B} - B}{\psi - \theta\tilde{\psi}}\mathbf{v},$$

which, when filled into (5.5b), yields

$$(5.7) \quad -\psi\mathbf{v} + B^\top \frac{\theta\tilde{B} - B}{\psi - \theta\tilde{\psi}}\mathbf{v} = \theta(\tilde{B}\mathbf{v} + \tilde{\psi} \frac{\theta\tilde{B} - B}{\psi - \theta\tilde{\psi}}\mathbf{v}).$$

After left-multiplying by  $\mathbf{v}^*$ , this can be manipulated into a quadratic equation in  $\theta$ :

$$(5.8) \quad \begin{aligned} a\theta^2 - b\theta + c &:= \mathbf{v}^*(\tilde{B}^\top\tilde{B} + \tilde{\psi}^2I)\mathbf{v}\theta^2 \\ &\quad - \mathbf{v}^*(B^\top\tilde{B} + 2\psi\tilde{\psi}I + \tilde{B}^\top B)\mathbf{v}\theta \\ &\quad + \mathbf{v}^*(B^\top B + \psi^2I)\mathbf{v} = 0. \end{aligned}$$

Note that  $a$ ,  $b$ , and  $c$  are real numbers due to the matrices between parentheses being real and symmetric. The solutions to (5.8) are found as

$$(5.9) \quad \theta_\pm = \frac{b}{2a} \pm \sqrt{\left(\frac{b}{2a}\right)^2 - \frac{c}{a}} =: \Re(\theta) \pm i\Im(\theta).$$

Later, Lemma 5.2 will prove that  $\left(\frac{b}{2a}\right)^2 - \frac{c}{a} \leq 0$  always holds. We can then state  $\Re(\theta)^2 = \left(\frac{b}{2a}\right)^2$  and  $\Im(\theta)^2 = \frac{c}{a} - \left(\frac{b}{2a}\right)^2$ . It holds that

$$\begin{aligned}
|1 - \theta|^2 &= \Re(1 - \theta)^2 + \Im(1 - \theta)^2 = (1 - \Re(\theta))^2 + \Im(\theta)^2 \\
&= \left(1 - \frac{b}{2a}\right)^2 + \left(\frac{c}{a} - \left(\frac{b}{2a}\right)^2\right) = 1 + \frac{c}{a} - \frac{b}{a} \\
(5.10) \quad &= \frac{\mathbf{v}^*(B^\top B + \tilde{B}^\top \tilde{B} - B^\top \tilde{B} - \tilde{B}^\top B + \psi^2 I + \tilde{\psi}^2 I - 2\psi\tilde{\psi}I)\mathbf{v}}{\mathbf{v}^*(\tilde{B}^\top \tilde{B} + \tilde{\psi}^2 I)\mathbf{v}} \\
&= \frac{\mathbf{v}^*((B - \tilde{B})^\top (B - \tilde{B}) + (\psi - \tilde{\psi})^2 I)\mathbf{v}}{\mathbf{v}^*(\tilde{B}^\top \tilde{B} + \tilde{\psi}^2 I)\mathbf{v}},
\end{aligned}$$

which is exactly (5.3).  $\square$

LEMMA 5.2. *In the quadratic equation (5.8), it always holds that*

$$(5.11) \quad b^2 - 4ac \leq 0.$$

*Proof.* We normalize  $\mathbf{v}$  without loss of generality. By defining  $\mathbf{v}_1 := \tilde{B}^\top \mathbf{v}$  and  $\mathbf{v}_2 := B^\top \mathbf{v}$ , we can write

$$(5.12) \quad a = \mathbf{v}_1^* \mathbf{v}_1 + \tilde{\psi}^2, \quad b = 2\mathbf{v}_2^* \mathbf{v}_1 + 2\psi\tilde{\psi}, \quad \text{and} \quad c = \mathbf{v}_2^* \mathbf{v}_2 + \psi^2.$$

Define  $\hat{\mathbf{v}}_1$  by appending  $\tilde{\psi}$  to  $\mathbf{v}_1$  and  $\hat{\mathbf{v}}_2$  by doing the same with  $\psi$  and  $\mathbf{v}_2$ . Then the expression  $b^2 - 4ac$  is equal to

$$(5.13) \quad 4\langle \hat{\mathbf{v}}_1, \hat{\mathbf{v}}_2 \rangle^2 - 4\langle \hat{\mathbf{v}}_1, \hat{\mathbf{v}}_1 \rangle \langle \hat{\mathbf{v}}_2, \hat{\mathbf{v}}_2 \rangle = 4(\cos^2(\omega) - 1)\langle \hat{\mathbf{v}}_1, \hat{\mathbf{v}}_1 \rangle \langle \hat{\mathbf{v}}_2, \hat{\mathbf{v}}_2 \rangle,$$

with  $\omega$  the angle between  $\hat{\mathbf{v}}_1$  and  $\hat{\mathbf{v}}_2$ . Since  $-1 \leq \cos(\omega) \leq 1$ , the lemma holds.  $\square$

Having proven the general Lemma 5.1, we can fill in our particular  $B$  and  $\tilde{B}$  matrices. If  $(1 - \theta)$  is an eigenvalue of  $S_\sigma$ , it holds that, for some  $\mathbf{v}$ ,

$$(5.14) \quad |1 - \theta|^2 = \frac{\mathbf{v}^* M_1 \mathbf{v} + \|\mathbf{v}\|_2^2 (\psi - \tilde{\psi})^2}{\mathbf{v}^* M_2 \mathbf{v} + \|\mathbf{v}\|_2^2 \tilde{\psi}^2}$$

with

$$(5.15) \quad M_1 = \begin{bmatrix} (\tilde{\varphi} - \varphi)^2 & & & \\ & \ddots & & \\ & & (\tilde{\varphi} - \varphi)^2 & \\ & & & 0 \end{bmatrix} \quad \text{and} \quad M_2 = \begin{bmatrix} 1 + \tilde{\varphi}^2 & -\tilde{\varphi} & & \\ -\tilde{\varphi} & \ddots & \ddots & \\ & \ddots & \ddots & 1 + \tilde{\varphi}^2 - \tilde{\varphi} \\ & & -\tilde{\varphi} & 1 \end{bmatrix}.$$

We can normalize  $\mathbf{v}$  such that  $\|\mathbf{v}\|_2 = 1$  without altering the value of  $|1 - \theta|$ . Then

$$\begin{aligned}
(5.16) \quad |1 - \theta|^2 &= \frac{\mathbf{v}^* M_1 \mathbf{v} + (\psi - \tilde{\psi})^2}{\mathbf{v}^* M_2 \mathbf{v} + \tilde{\psi}^2} \leq \frac{(\tilde{\varphi} - \varphi)^2 + (\psi - \tilde{\psi})^2}{\mathbf{v}^* M_2 \mathbf{v} + \tilde{\psi}^2} \\
&< \frac{(\tilde{\varphi} - \varphi)^2 + (\psi - \tilde{\psi})^2}{(1 - \tilde{\varphi})^2 + \tilde{\psi}^2}.
\end{aligned}$$

The first inequality is valid since  $\mathbf{v}^* M_1 \mathbf{v} = (1 - |v_{\tilde{L}}|^2)(\tilde{\varphi} - \varphi)^2 \leq (\tilde{\varphi} - \varphi)^2$ , where  $0 \leq |v_{\tilde{L}}| \leq 1$  is the magnitude of the last element in  $\mathbf{v}$ . The second inequality is more involved, and is proven by the following lemma. Then, (5.16) proves Theorem 3.10.

LEMMA 5.3. *Any eigenvalue  $\xi$  of  $M_2$ , defined in (5.15), satisfies  $\xi > (1 - \tilde{\varphi})^2$ .*

*Proof.* From [15, Theorem 4], one can deduce that the matrix

$$(5.17) \quad \widehat{M}_2 := \begin{bmatrix} 1+\tilde{\varphi}^2 & -\tilde{\varphi} & & & \\ -\tilde{\varphi} & 1+\tilde{\varphi}^2 & \ddots & & \\ & \ddots & \ddots & \ddots & \\ & & & & -\tilde{\varphi} \\ -\tilde{\varphi} & 1-\tilde{\varphi}+\tilde{\varphi}^2 & & & \end{bmatrix}$$

has eigenvalues

$$(5.18) \quad \widehat{\xi}_j = 1 + \tilde{\varphi}^2 + 2\tilde{\varphi} \cos \frac{2j\pi}{2\widehat{L} + 1}, \quad j = 1, \dots, \widehat{L},$$

which means  $\widehat{\xi}_j > (1 - \tilde{\varphi})^2$ . To transform  $\widehat{M}_2$  into  $M_2$ , one adds  $(\tilde{\varphi} - \tilde{\varphi}^2)$  to the last diagonal element. Since this is a positive number (Assumption 3.3 ensures that  $0 < \tilde{\varphi} < 1$ ), it cannot reduce the minimum eigenvalue of this symmetric matrix (as follows from [17, Theorem 10.3.1]). This proves the lemma.  $\square$

**6. Proof of Theorem 3.12.** Given the discussion in subsection 3.1 it holds that  $\rho = \max_{\sigma \in \text{eig}(K)} \max(|\text{eig}(S_\sigma)|)$ , with  $S_\sigma$  given by (3.9b). Define  $B$  and  $\tilde{B}$  such that

$$(6.1) \quad S_\sigma = I - \begin{bmatrix} \tilde{B} & \tilde{\psi}I \\ -E & \tilde{B}^\top \end{bmatrix}^{-1} \begin{bmatrix} B & \psi I \\ -E & B^\top \end{bmatrix},$$

where  $E$  is all-zero except for a one in the bottom-right corner. This is analogous to the proof in section 5. However, we have no equivalent of Lemma 5.2, so we will need to deal with separate cases for non-real and real eigenvalues of (6.1).

*Non-real eigenvalues.* We start by looking at the non-real case.

LEMMA 6.1. *Let  $\theta$  be an eigenvalue with non-zero imaginary part of*

$$(6.2) \quad \begin{bmatrix} \tilde{B} & \tilde{\psi}I \\ -E & \tilde{B}^\top \end{bmatrix}^{-1} \begin{bmatrix} B & \psi I \\ -E & B^\top \end{bmatrix}$$

with  $B, \tilde{B} \in \mathbb{R}^{\widehat{L} \times \widehat{L}}$  and where  $E$  is as in (6.1). Then, for some vector  $\mathbf{v} \in \mathbb{C}^{\widehat{L}}$ ,

$$(6.3) \quad |1 - \theta|^2 = \frac{\mathbf{v}^*((B - \tilde{B})(B - \tilde{B})^\top)\mathbf{v}}{\mathbf{v}^*(\tilde{B}\tilde{B}^\top + \tilde{\psi}E)\mathbf{v}}.$$

*Proof.* The proof is similar to that of Lemma 5.1. We introduce an eigenvalue  $\theta$  and its corresponding eigenvector  $(\mathbf{v}^\top, \mathbf{w}^\top)^\top$ , such that

$$(6.4a) \quad B\mathbf{v} + \psi\mathbf{w} = \theta(\tilde{B}\mathbf{v} + \tilde{\psi}\mathbf{w}),$$

$$(6.4b) \quad -E\mathbf{v} + B^\top\mathbf{w} = \theta(-E\mathbf{v} + \tilde{B}^\top\mathbf{w}),$$

and thus  $\mathbf{w} = \frac{\theta\tilde{B} - B}{\psi - \theta\tilde{\psi}}\mathbf{v}$ . After filling this into (6.4b) and left-multiplying by  $\mathbf{v}^*$ , we can manipulate everything into the quadratic equation

$$(6.5) \quad \begin{aligned} a\theta^2 - b\theta + c &:= \mathbf{v}^*(\tilde{B}^\top\tilde{B} + \tilde{\psi}E)\mathbf{v}\theta^2 \\ &\quad - \mathbf{v}^*(B^\top\tilde{B} + (\psi + \tilde{\psi})E + \tilde{B}^\top B)\mathbf{v}\theta \\ &\quad + \mathbf{v}^*(B^\top B + \psi E)\mathbf{v} = 0 \end{aligned}$$

with solution  $\theta_\pm = \frac{b}{2a} \pm \sqrt{\left(\frac{b}{2a}\right)^2 - \frac{c}{a}}$ .

Since we look for solutions  $\theta$  with non-zero imaginary part, the contents of the square root must be negative. Then, similarly to before,

$$(6.6) \quad |1 - \theta|^2 = 1 + \frac{c}{a} - \frac{b}{a} = \frac{\mathbf{v}^*((B - \tilde{B})^\top(B - \tilde{B}))\mathbf{v}}{\mathbf{v}^*(\tilde{B}^\top\tilde{B} + \tilde{\psi}E)\mathbf{v}}. \quad \square$$

We utilize this lemma in the same way as before, but now must keep in mind that its result is only guaranteed for non-real eigenvalues. In that case, we can state

$$(6.7) \quad |1 - \theta| = \sqrt{\frac{\mathbf{v}^*M_1\mathbf{v}}{\mathbf{v}^*M_2\mathbf{v} + \tilde{\psi}|v_{\tilde{L}}|^2}} \leq \frac{|\varphi - \tilde{\varphi}|}{1 - \tilde{\varphi}}$$

where we recall  $M_1$  and  $M_2$  from (5.15).

*Real eigenvalues.* When the contents of the square root in (6.4)'s solution are non-negative, the reasoning breaks down. This case can be treated in a different way. By left-multiplying (6.4a) and (6.4b) by  $\mathbf{w}^*$  and  $\mathbf{v}^*$ , respectively, and then subtracting the complex adjoint of the latter from the former, we find that

$$(6.8) \quad \mathbf{w}^*\psi\mathbf{w} + \mathbf{v}^*E\mathbf{v} = \theta(\mathbf{w}^*\tilde{\psi}\mathbf{w} + \mathbf{v}^*E\mathbf{v}) \Leftrightarrow \theta = \frac{\psi\|\mathbf{w}\|_2^2 + |v_{\tilde{L}}|^2}{\tilde{\psi}\|\mathbf{w}\|_2^2 + |v_{\tilde{L}}|^2},$$

such that, shifting our focus to  $(1 - \theta)$ , we obtain

$$(6.9) \quad (1 - \theta) = \frac{(\tilde{\psi} - \psi)\|\mathbf{w}\|_2^2}{\tilde{\psi}\|\mathbf{w}\|_2^2 + |v_{\tilde{L}}|^2}.$$

As shown in [5, (3.24) and (3.28)], it holds that  $v_{\tilde{L}} = w_{\tilde{L}}$  and  $w_l = w_{\tilde{L}}(\tilde{\varphi} + \frac{\varphi - \tilde{\varphi}}{1 - \theta})^{\tilde{L}-l}$ . A normalization such that  $w_{\tilde{L}} = 1$  and the definition  $x := (1 - \theta)$  then yield

$$(6.10) \quad x = \frac{\tilde{\psi} - \psi}{\tilde{\psi} + 1/\sum_{l=0}^{\tilde{L}-1}(\tilde{\varphi} + \frac{\varphi - \tilde{\varphi}}{x})^{2l}} \Leftrightarrow f_{\tilde{L}}(x) := \frac{\tilde{\psi} - \psi}{\tilde{\psi} + 1/\sum_{l=0}^{\tilde{L}-1}(\tilde{\varphi} + \frac{\varphi - \tilde{\varphi}}{x})^{2l}} - x = 0.$$

Define  $g(x) := (\tilde{\psi} - \psi)/\tilde{\psi} - x$ . We have, depending on  $\text{sign}(\tilde{\psi} - \psi)$ ,

$$(6.11) \quad \forall x : f_{\tilde{L}}(x) \leq f_\infty(x) \leq g(x) \quad \text{or} \quad \forall x : f_{\tilde{L}}(x) \geq f_\infty(x) \geq g(x).$$

Now denote by  $x_1$  a root of  $f_{\tilde{L}}$ , and by  $x_2$  the root of  $g$ . Clearly,

$$(6.12) \quad \text{sign}(x_1) = \text{sign}(x_2) \quad \text{and} \quad |x_1| \leq |x_2|.$$

This means that  $\min\{f_\infty(x_1), f_\infty(x_2)\} \leq 0 \leq \max\{f_\infty(x_1), f_\infty(x_2)\}$ . Since  $f_{\tilde{L}}$ ,  $f_\infty$ , and  $g$  are continuous, Bolzano's theorem asserts that

$$(6.13) \quad f_\infty(x^*) = 0 \quad \text{for some} \quad \min\{x_1, x_2\} \leq x^* \leq \max\{x_1, x_2\},$$

which, by (6.12), means that  $|x^*| \geq |x_1|$ . Recall that any *real* eigenvalue  $x = (1 - \theta)$  of the ParaOpt iteration matrix must be a root of  $f_{\tilde{L}}$ ; by the above argument, then,  $|1 - \theta|$  is bounded from above by the absolute value of at least one root of

$$(6.14) \quad f_\infty(x) = \frac{\tilde{\psi} - \psi}{\tilde{\psi} + 1/\sum_{l=0}^{\infty}(\tilde{\varphi} + \frac{\varphi - \tilde{\varphi}}{x})^{2l}} - x.$$

This root is efficiently computable: if  $x = (\tilde{\psi} - \psi)/\tilde{\psi}$  makes the infinite sum diverge, it is a root (and the one with the largest absolute value). Otherwise, all roots must have the sum converge, which can then be replaced by  $(1 - (\tilde{\varphi} + \frac{\varphi - \tilde{\varphi}}{x})^2)^{-1}$ . Then finding  $f_\infty$ 's roots amounts to solving a quadratic equation and checking when the sum converges. Our numerical tests suggest that  $f_\infty$  always has exactly one root.



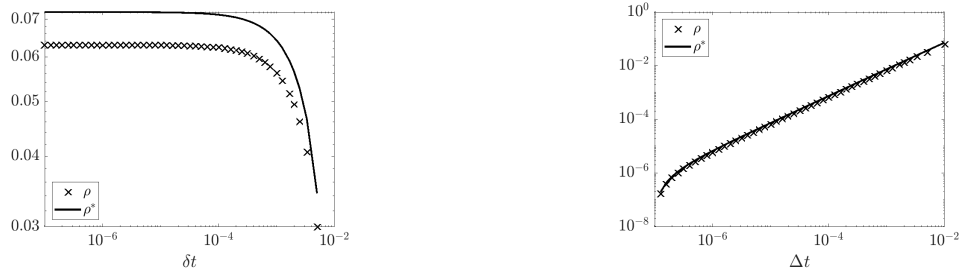


Fig. 7.1: Spectral radius  $\rho$  and bound  $\rho^*$  from (3.17) of the ParaOpt iteration matrix for a fixed coarse time step  $\Delta t = \Delta T$  (left) and a fixed fine time step  $\delta t = 10^{-5}\Delta T$  (right), for the tracking problem with implicit-Euler propagators from subsection 7.1

**7. Numerical results.** Section 3 presents upper bounds on the ParaOpt convergence factor for linear diffusive problems. Subsections 7.1 and 7.2 will study the accuracy and sharpness of these bounds through numerical tests. Later, subsection 7.3 looks at the performance of the proposed preconditioners.

Our tests confirm the accuracy of our bounds and the scalability of preconditioned ParaOpt. To perform them, we have extended the `pintopt` package<sup>1</sup> designed in [2] to include a sequential implementation of ParaOpt and its preconditioners. Though unoptimized, it is a useful reference solver and can be used to study iteration counts.

**7.1. Assessing the bounds for tracking.** Consider the scalar equation

$$(7.1) \quad y'(t) = -\sigma y(t) + u(t), \quad y(0) = y_{\text{init}}$$

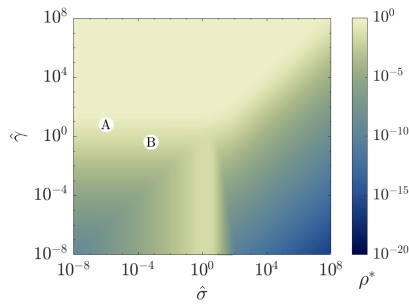
with a tracking objective function, analogously to a test case in [5]. We follow [5] in setting  $\gamma = 1$ ,  $\sigma = 16$  and  $T = 1$  and compare the true spectral radius  $\rho$  of ParaOpt's iteration matrix (3.9) to the bound  $\rho^*$  set by (3.17).

Figure 7.1 uses  $\widehat{L} = 100$  and looks at the influence of the time steps. In the left figure, the coarse step  $\Delta t = \Delta T$  is kept fixed and the fine one  $\delta t$  is varied. The bound  $\rho^*$  is correct and rather sharp, and  $\rho$  becomes steady since  $\delta t \rightarrow 0$  corresponds to the limit of an exact solver. The right figure fixes the fine time step  $\delta t = 10^{-5}\Delta T$  and varies the coarse one. Expectedly, a small coarse time step leads to faster convergence.

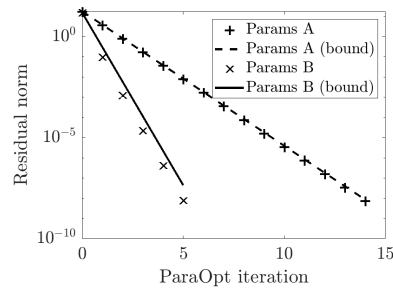
To confirm that this spectral radius has the impact on convergence expected from subsection 3.1, ParaOpt has been executed on two scalar problems. Both use  $L = 50$  and  $T = 50$ , with  $y_{\text{init}} = y_{\text{d}}(\cdot) = 1$ . The fine propagator is exact while the coarse one uses 10 steps of implicit Euler. The parameter sets, called A and B, are displayed in Figure 7.2a: case A uses  $\widehat{\sigma} = 10^{-6}$  and  $\widehat{\gamma} = 6$ , while case B uses  $\widehat{\sigma} = 0.0006$  and  $\widehat{\gamma} = 0.4$ . They are overlaid on a copy of Figure 3.1b, which shows  $\rho^*$  for these propagators. Parameters B lead to a smaller  $\rho^*$ , so ParaOpt may be expected to converge faster for that problem than for A; Figure 7.2b confirms this. In addition, the residuals decrease at a rate close to the bound, confirming its accuracy.

Next, consider the weak-scaling regimes from subsection 4.1. We use an exact fine propagator and a one-step implicit-Euler coarse one. Recall that the upper bound is  $\widehat{L}$ -independent, which guarantees weak scalability for fixed  $\Delta T$ . Figure 7.3a confirms the bound is sharp. For fixed  $T$  (i.e., decreasing  $\Delta T$ ), Figure 7.3b shows good scalability.

<sup>1</sup>The version of the `pintopt` MATLAB package used here and code to reproduce our results are located at <https://gitlab.kuleuven.be/numa/public/pintopt>. To keep this paper reproducible, new additions and bugfixes are tracked only at <https://github.com/ArneBouillon/pintopt>.

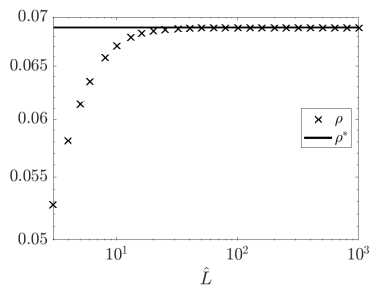


(a)  $\rho^*$  for parameter choices A and B

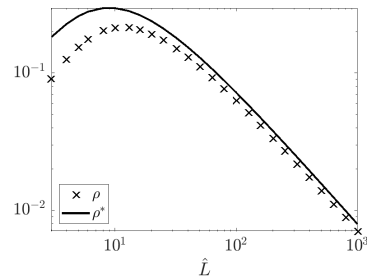


(b) True convergence and rate (3.17)

Fig. 7.2: Scalar tracking ParaOpt with exact  $\mathcal{P}/\mathcal{Q}$  and 10-step implicit-Euler  $\tilde{\mathcal{P}}/\tilde{\mathcal{Q}}$ , using the parameters from subsection 7.1



(a) Fixed sub-interval size  $\Delta T = 1$



(b) Fixed total interval size  $T = 1$

Fig. 7.3: Spectral radius  $\rho$  and bound  $\rho^*$  from (3.17) of the tracking ParaOpt iteration matrix, using the parameters from subsection 7.1

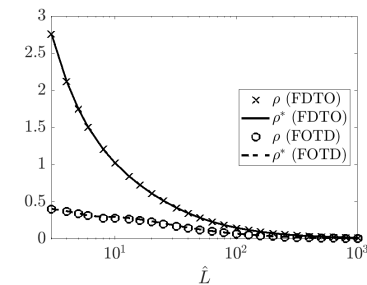
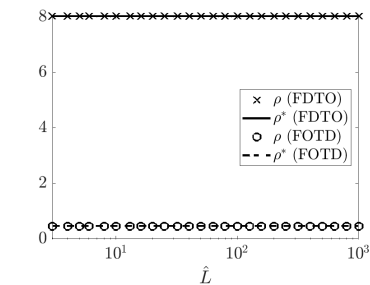
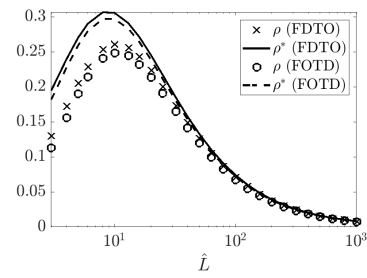
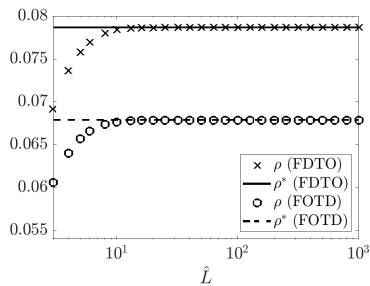


Fig. 7.4: Equivalents of Figure 7.3 for terminal cost with  $\gamma = 1$  (first row) and  $\gamma = 1e-6$  (second row)

**7.2. Assessing the bounds for terminal cost.** The experiments in subsection 7.1 can be repeated for the terminal-cost case, with the target trajectory  $y_d(\cdot) = 1$  replaced by a target state  $y_{\text{target}} = 1$ . In a bid not to qualitatively repeat experiments from [5], we focus on the main difference between our results: the switch from FDTO to FOTD for the coarse propagator, whose analysis is enabled by our more general convergence bound in Theorem 3.12. Figure 7.4 repeats the scaling test from Figure 7.3 in the terminal-cost setting. We compare a medium  $\gamma = 1$  to a very small  $\gamma = 10^{-6}$  (that is, a large  $\hat{\gamma}$ , meaning control is cheap). As expected from Figure 3.2, FOTD and FDTO differ little in the former case and a lot in the latter. Herein lies the advantage of the FOTD implicit-Euler coarse propagator: ParaOpt converges for all linear diffusive problems, not just those with sufficiently small time steps.

**7.3. Preconditioning.** As discussed in subsection 4.1, the two main processes to study in ParaOpt are the outer inexact-Newton iterations and the inner linear-system solves that constitute the inexact-Newton corrections. The past two subsections have confirmed the scalability of the former – now, we verify whether the proposed preconditioners succeed in completing the picture by keeping inner iterations constant when the number of parallel time intervals is scaled.

*Heat problem.* We study the same heat problem considered in [2] (and loosely adapted from [3]), defined on a periodic spatial domain  $\Omega = [0, 1]^2$  and given by

$$(7.2) \quad \partial_t y = \Delta y + u,$$

where the spatial derivative is discretized using central differences. We also use [2]’s initial value, target trajectory and target state

$$\begin{aligned} y_{\text{init}}(x) &= \frac{1}{12\pi^2\gamma}(1 - T)\text{sign}(\sin(2\pi x_1))\sin^2(2\pi x_2) \\ y_{\text{target}}(x) &= \sin(2\pi x_1)\sin(2\pi x_2) \\ y_d(t, x) &= \left( (12\pi^2 + (12\pi^2\gamma)^{-1})(t - T) - (1 + ((12\pi^2)^2\gamma)^{-1}) \right) \sin(2\pi x_1)\sin(2\pi x_2). \end{aligned}$$

A non-smooth  $y_{\text{init}}$  is important to make the preconditioning problem sufficiently challenging, as also noticed in [8, 23]. We use the same parameters  $\gamma = 0.05$  and  $T = 2$  as [9], and a spatial grid of  $M = 8 \times 8$  points (a small value, to keep the non-preconditioned computation tractable). The fine propagator uses 10 implicit-Euler steps; the coarse one just 1. All further results will use a tolerance of  $10^{-6}$  for ParaOpt, and will employ a GMRES inner solver with a tolerance of  $10^{-4}$ .

*Remark 7.1* (ParaOpt’s inner GMRES tolerance). A significant difference between ParaDiag’s use as a stand-alone method and its adaptation as a ParaOpt preconditioner is the tolerance to which the system should be solved. Since ParaOpt solves a system with a Jacobian that is already approximate, there is no need to solve the system to full precision. Figure 7.5 shows that, for the heat problem we are about to study with  $\hat{L} = 10$ ,  $T = 2$ ,  $\gamma = 0.05$ ,  $M = 8 \times 8$ , a ten-step fine and a one-step coarse implicit-Euler propagator, a tolerance as high as  $10^{-3}$  already performs well.

Figure 7.6 shows how many GMRES iterations are required within each ParaOpt iteration for  $\hat{L} \in \{10, 100\}$ . Using the preconditioner, this number is not only much lower, but also remains virtually constant when  $\hat{L}$  changes. The difference preconditioning makes is seen even more strikingly in Figure 7.7, which sums up the GMRES iterations over all ParaOpt iterations. Using our preconditioners, the work per processor remains constant when scaling the processors in tandem with  $\hat{L}$  – in other words, the algorithm is weakly scalable.

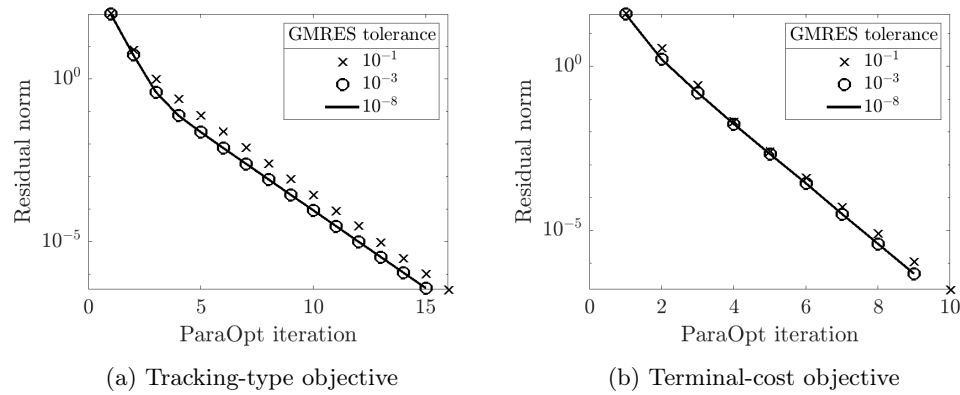


Fig. 7.5: Heat problem ParaOpt residual, for different GMRES tolerances

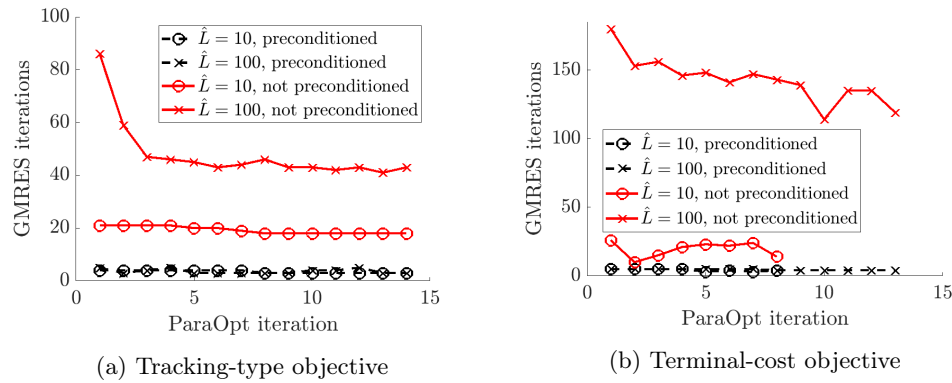


Fig. 7.6: (Un)preconditioned GMRES iteration counts for the heat problem

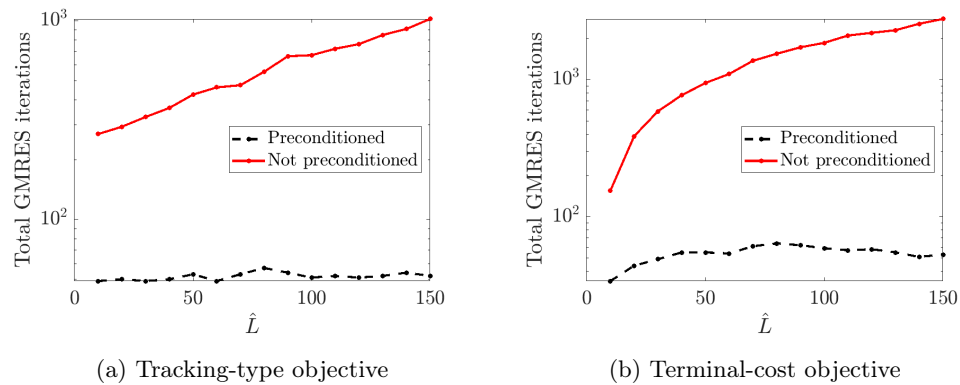


Fig. 7.7: (Un)preconditioned total GMRES iteration counts for the heat problem

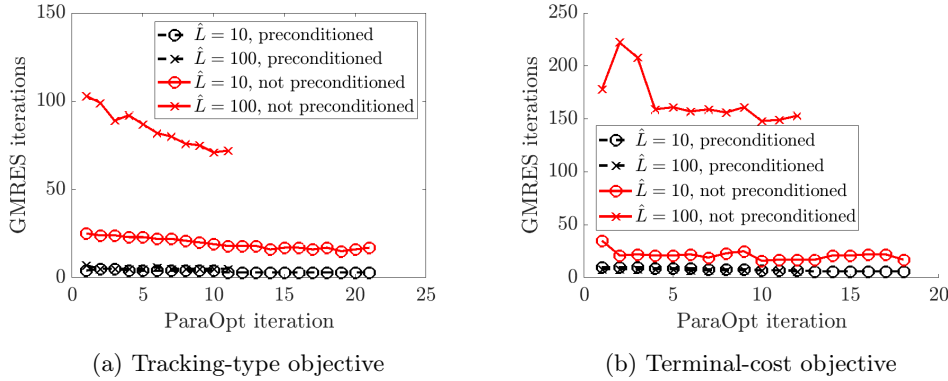


Fig. 7.8: (Un)preconditioned GMRES iteration counts for the advection-diffusion problem

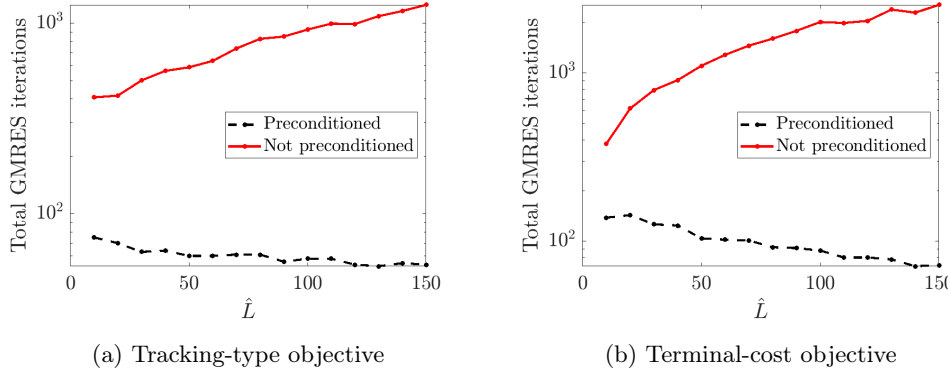


Fig. 7.9: (Un)preconditioned total GMRES iteration counts for the advection-diffusion problem

*Advection-diffusion problem.* In addition to the diffusion problem which follows the theory in section 3 and [2], we study an advection-diffusion problem. Its  $K$  matrix is not symmetric, such that our theory does not apply – however, the preconditioners from section 4 can still be used. Consider the equation

$$(7.3) \quad \partial_t y = \frac{\Delta y}{10} - \partial_{x_1} y - \partial_{x_2} y + u.$$

which retains some diffusion (otherwise, ParaOpt itself might have poor convergence, unrelated to the preconditioners) but adds an advection term. We use the same  $y_d$ ,  $y_{\text{target}}$ , and  $y_{\text{init}}$  as for the heat problem and again discretize spatial derivatives using central differences. Figures 7.8 and 7.9 are the advection-diffusion counterparts to Figures 7.6 and 7.7, to which they are qualitatively very similar. We can conclude that the proposed preconditioner performs well, even outside the regime where it is fully understood. A similar conclusion was drawn in the ParaDiag context [2].

**8. Conclusions.** The main focus of this paper is on linear diffusive problems. In that setting, and when Assumptions 3.1 to 3.3 are satisfied, we adapted ParaOpt to work for both tracking and terminal-cost objectives, additionally proposing generic convergence bounds and a preconditioner that ensures good weak scalability. We summarize our main contributions in the linear diffusive setting.

- We formulated an extension of ParaOpt to the setting of tracking problems.
- We proved a generalized convergence bound for terminal-cost ParaOpt that is generic in the propagators used (as long as they satisfy Assumptions 3.1 to 3.3). Numerical results confirmed the bound’s validity and showed that it is even sharper than the state-of-the-art result [5].
- We proved a similar bound for the tracking setting and proved that the case of an exact fine and a one-step implicit-Euler coarse propagator guarantees ParaOpt does not diverge.
- Thanks to the generic convergence bound, we were able to study a different type of implicit-Euler coarse propagator for terminal-cost problems and found that it improves ParaOpt’s convergence.
- We proposed diagonalization-based preconditioners to improve the scaling of ParaOpt. Analytic results from the ParaDiag literature and numerical tests confirm that ParaOpt is now a weakly scalable algorithm.

For problems outside the linear diffusive category, ParaOpt is still a very promising method [5], although poorly understood. Our preconditioners apply as long as the coarse propagator is affine in its arguments, even for non-diffusive and non-symmetric problems. In addition, we are confident that these preconditioners can be extended to non-linear coarse propagators, although we leave this for future work. Recall that our application of diagonalization-based preconditioners to ParaOpt was inspired by proceedings in [22] for the IVP Parareal algorithm. There, non-linear Parareal is supported by using non-linear variants of ParaDiag. For IVPs, these non-linear ParaDiag methods exist [4, 14]. Developing similar techniques for optimization ParaDiag would open the way for preconditioning non-linear ParaOpt similarly to what we proposed.

Other interesting future work could consist of applying ParaOpt to realistic applications, testing the proposed preconditioners on more complex (but still linear) problems. In addition, with the generic bounds in subsection 3.2, the search for coarse propagators with better convergence properties than implicit Euler is wide open: one simply needs to calculate a propagator’s  $\tilde{\varphi}$  and  $\tilde{\psi}$  (see Appendix A.1) to evaluate its performance.

We conclude by noting that ParaOpt does not necessarily need a parallel preconditioner; the fine propagations can already be parallelized, so as long as the coarse-grid correction is cheap, it need not be parallel for the method itself to achieve speed-ups (in fact, the base version of Parareal has sequential coarse-grid correction). It would therefore be feasible for sequential preconditioners to match or surpass the performance of the ones proposed here, if they cause the system to be solved in fewer iterations.

**Appendix A. Properties of some ParaOpt propagators.** This appendix contains calculations for various properties of the ParaOpt propagators in section 3.

**A.1. On  $\varphi$  and  $\psi$ , and how to find them.** Consider a time interval  $[T_{l-1}, T_l]$  with  $T_l - T_{l-1} = \Delta T$ . Then the tracking propagators  $\mathcal{P}(\mathbf{y}_{l-1}, \widehat{\lambda}_l)$  and  $\mathcal{Q}(\mathbf{y}_{l-1}, \widehat{\lambda}_l)$  for a linear diffusive system approximately solve the system

$$(A.1a) \quad \mathbf{y}'(t) = -K\mathbf{y}(t) - \widehat{\lambda}(t)/\sqrt{\gamma}, \quad \mathbf{y}(T_{l-1}) = \mathbf{y}_{l-1},$$

$$(A.1b) \quad \widehat{\lambda}'(t) = (\mathbf{y}_d(t) - \mathbf{y}(t))/\sqrt{\gamma} + K\widehat{\lambda}(t), \quad \widehat{\lambda}(T_l) = \widehat{\lambda}_l.$$

Assumptions 3.1 and 3.2 can now be checked, either by reasoning about the discretization scheme or by fully calculating  $\Phi$  and  $\Psi$ . In the former case, the eigenvalues  $\varphi$  and  $\psi$  can then be found by considering the scalar problem

$$(A.2a) \quad y'(t) = -\sigma y(t) - \widehat{\lambda}(t)/\sqrt{\gamma}, \quad y(T_{l-1}) = y_{l-1}$$

$$(A.2b) \quad \widehat{\lambda}'(t) = (y_d(t) - y(t))/\sqrt{\gamma} + \sigma\widehat{\lambda}(t), \quad \widehat{\lambda}(T_l) = \widehat{\lambda}_l.$$

A discretization of (A.2) and one of the expressions

$$(A.3a) \quad y(T_l) \approx \mathcal{P}(y_{l-1}, \widehat{\lambda}_l) = \varphi y_{l-1} - \psi \widehat{\lambda}_l + b_{\mathcal{P},l},$$

$$(A.3b) \quad \widehat{\lambda}(T_{l-1}) \approx \mathcal{Q}(y_{l-1}, \widehat{\lambda}_l) = \psi y_{l-1} + \varphi \widehat{\lambda}_l + b_{\mathcal{Q},l}$$

together yield  $\varphi$  and  $\psi$ . An analogous procedure can be employed for terminal cost.

**A.2. Proof of Lemma 3.5.** It is clear that Assumptions 3.1 and 3.2 hold for an FOTD implicit-Euler discretization of (A.1), which discretizes the state equation forward in time with implicit Euler and the adjoint equation backward. Indeed, affinity and simultaneous diagonalizability follow from the fact that the discretization can be written as a large linear system using only  $K$  and scaled identity matrices, while the rest of Assumption 3.2 follows from the symmetry of (A.1) and the discretization.

When using implicit Euler with  $J$  steps to discretize the system (A.2), let us – with a slight abuse of notation – introduce new indices  $j$  on  $y$  and  $\lambda$ . The starting index  $(l-1)$  becomes  $j=0$ ,  $l$  becomes  $j=J$ , and intermediate  $j$  values are used for the finer grid of implicit Euler. The time step is  $\tau = \Delta T/J$ . Define  $\zeta := (1 + \sigma\tau)$ , such that the implicit-Euler discretization reads (for  $j = 1, \dots, J$ )

$$(A.4a) \quad y_j - \zeta^{-1}y_{j-1} + \tau\zeta^{-1}\widehat{\lambda}_j/\sqrt{\gamma} = 0,$$

$$(A.4b) \quad \widehat{\lambda}_{j-1} - \zeta^{-1}\widehat{\lambda}_j - \tau\zeta^{-1}y_{j-1}/\sqrt{\gamma} = -\tau\zeta^{-1}y_{d,j-1}/\sqrt{\gamma}.$$

Let us now define  $\varphi_\tau^{(j)}$  and  $\psi_\tau^{(j)}$  as the  $\varphi$  and  $\psi$  for  $j$  length- $\tau$  steps – then the variables we are looking for are  $\varphi_\tau^{(J)}$  and  $\psi_\tau^{(J)}$ . For any  $j$ , we can write

$$(A.5) \quad -\varphi_\tau^{(j)}y_0 + y_j + \psi_\tau^{(j)}\widehat{\lambda}_j = b_j \quad \text{for some } b_j.$$

This gives a base case  $\varphi_\tau^{(0)} = 1$  and  $\psi_\tau^{(0)} = 0$ . Now suppose that  $\varphi_\tau^{(j)}$  and  $\psi_\tau^{(j)}$  are known for some  $j$ . Combining (A.5) (for  $j+1$ ) with the discretization (A.4) gives

$$\begin{aligned} & -\varphi_\tau^{(j+1)}y_0 + y_{j+1} + \psi_\tau^{(j+1)}\widehat{\lambda}_{j+1} = b_{j+1} \\ \Leftrightarrow & \quad -\varphi_\tau^{(j+1)}y_0 + (\zeta^{-1}y_j - \widehat{\gamma}_\tau\zeta^{-1}\widehat{\lambda}_{j+1}) + \psi_\tau^{(j+1)}\widehat{\lambda}_{j+1} = b_{j+1} \\ \Leftrightarrow & \quad -\varphi_\tau^{(j+1)}y_0 + \zeta^{-1}y_j + (\psi_\tau^{(j+1)} - \widehat{\gamma}_\tau\zeta^{-1})(\zeta\widehat{\lambda}_j - \widehat{\gamma}_\tau y_j) = \widehat{b}_{j+1} \\ \Leftrightarrow & \quad -\varphi_\tau^{(j+1)}y_0 + (\zeta^{-1} - \widehat{\gamma}_\tau(\psi_\tau^{(j+1)} - \widehat{\gamma}_\tau\zeta^{-1}))y_j + (\psi_\tau^{(j+1)}\zeta - \widehat{\gamma}_\tau)\widehat{\lambda}_j = \widehat{b}_{j+1} \end{aligned}$$

for some  $\widehat{b}_j$ . Comparing this to (A.5), a few algebraic manipulations yield (3.12).

We should now check that Assumption 3.3 holds if  $\sigma > 0$ . The expression for  $\psi$  is clearly positive. We further have  $\varphi_\tau^{(0)} = 1$  and, for each subsequent  $j$ ,  $\varphi_\tau^{(j)}$  is equal to  $\varphi_\tau^{(j-1)}$  multiplied by a factor  $r^{(j)} := (\zeta^{-1} - \widehat{\gamma}(\psi_\tau^{(j)} - \widehat{\gamma}\zeta^{-1}))$ . We claim that  $0 < r^{(j)} < 1$  for  $j \geq 1$ , meaning that  $0 < \varphi_\tau^{(j)} < 1$  for  $j \geq 1$ . Indeed,

$$\begin{aligned} 0 < r^{(j)} < 1 &\Leftrightarrow 0 < 1 - \zeta\widehat{\gamma}(\psi_\tau^{(j)} - \widehat{\gamma}\zeta^{-1}) < \zeta \\ \Leftrightarrow (1 + \widehat{\gamma}^2)/(\zeta\widehat{\gamma}) > \psi_\tau^{(j)} > (1 + \widehat{\gamma}^2 - \zeta)/(\zeta\widehat{\gamma}) \\ \Leftrightarrow \frac{1 + \widehat{\gamma}^2}{\zeta\widehat{\gamma}} > \frac{\widehat{\gamma} + \zeta^{-1}(1 + \widehat{\gamma}^2)\psi_\tau^{(j-1)}}{\zeta + \widehat{\gamma}\psi_\tau^{(j-1)}} > \frac{1 + \widehat{\gamma}^2 - \zeta}{\zeta\widehat{\gamma}} \\ \Leftrightarrow \frac{1}{\zeta\widehat{\gamma}} > \frac{\psi_\tau^{(j-1)}}{\zeta^2 + \zeta\widehat{\gamma}\psi_\tau^{(j-1)}} > \frac{1 - \zeta}{\zeta\widehat{\gamma}}. \end{aligned}$$

These last inequalities hold; to see this, multiply the numerator and denominator of the leftmost expression by  $\psi_\tau^{(j-1)}$  and note that the rightmost expression is negative.

**A.3. Proof of Lemma 3.6.** For an exact solution to (A.1), note that

$$(A.6) \quad \begin{bmatrix} \mathbf{y}_l \\ \widehat{\boldsymbol{\lambda}}_l \end{bmatrix} = \exp\left(\Delta T \begin{bmatrix} -K & -I/\sqrt{\widehat{\gamma}} \\ -I/\sqrt{\widehat{\gamma}} & K \end{bmatrix}\right) \begin{bmatrix} \mathbf{y}_{l-1} \\ \widehat{\boldsymbol{\lambda}}_{l-1} \end{bmatrix} + \begin{bmatrix} \mathbf{v} \\ \mathbf{w} \end{bmatrix}$$

for some  $\mathbf{v}$  and  $\mathbf{w}$  (both dependent on  $\mathbf{y}_d$ ) that are of little importance here. Assumptions 3.1 and 3.2 follow easily from this expression. We can then consider the scalar case (by replacing  $K$  with  $\sigma$  and  $I$  with 1) and denote the matrix exponential in (A.6) as  $E =: \begin{bmatrix} \cdot & \cdot \\ \cdot & \cdot \end{bmatrix}$ . We obtain that  $\widehat{\boldsymbol{\lambda}}_l = c\mathbf{y}_{l-1} + d\widehat{\boldsymbol{\lambda}}_{l-1}$  and, thus,

$$(A.7) \quad \varphi = d^{-1} \quad \text{and} \quad \psi = -d^{-1}c.$$

To calculate  $E$ , finding  $c$  and  $d$ , denote  $M := \Delta T \begin{bmatrix} -\sigma & -1/\sqrt{\widehat{\gamma}} \\ -1/\sqrt{\widehat{\gamma}} & \sigma \end{bmatrix} = \begin{bmatrix} -\widehat{\sigma} & -\widehat{\gamma} \\ -\widehat{\gamma} & \widehat{\sigma} \end{bmatrix}$ . We define  $s := \sqrt{\widehat{\sigma}^2 + \widehat{\gamma}^2}$ . It can be checked that  $M = V\Sigma V^{-1}$  with

$$(A.8) \quad \Sigma = \begin{bmatrix} s & \\ & -s \end{bmatrix}, \quad V = \begin{bmatrix} \frac{\widehat{\sigma}-s}{\widehat{\gamma}} & \frac{\widehat{\sigma}+s}{\widehat{\gamma}} \\ 1 & 1 \end{bmatrix}, \quad \text{and} \quad V^{-1} = \begin{bmatrix} \frac{-\widehat{\gamma}}{2s} & \frac{\widehat{\sigma}+s}{2s} \\ \frac{\widehat{\gamma}}{2s} & \frac{-\widehat{\sigma}+s}{2s} \end{bmatrix}.$$

Then  $\exp(M) = V \exp(\Sigma) V^{-1}$ , where the exponential of a diagonal matrix can be distributed to its entries. We obtain

$$(A.9) \quad \begin{aligned} \exp(M) &= \begin{bmatrix} \frac{\widehat{\sigma}-s}{\widehat{\gamma}} & \frac{\widehat{\sigma}+s}{\widehat{\gamma}} \\ 1 & 1 \end{bmatrix} \begin{bmatrix} e^s & \\ & e^{-s} \end{bmatrix} \begin{bmatrix} \frac{-\widehat{\gamma}}{2s} & \frac{\widehat{\sigma}+s}{2s} \\ \frac{\widehat{\gamma}}{2s} & \frac{-\widehat{\sigma}+s}{2s} \end{bmatrix} \\ &= \begin{bmatrix} -e^s \frac{\widehat{\gamma}}{2s} \frac{\widehat{\sigma}-s}{\widehat{\gamma}} + e^{-s} \frac{\widehat{\gamma}}{2s} \frac{\widehat{\sigma}+s}{\widehat{\gamma}} & e^s \frac{\widehat{\sigma}+s}{2s} \frac{\widehat{\sigma}-s}{\widehat{\gamma}} + e^{-s} \frac{-\widehat{\sigma}+s}{2s} \frac{\widehat{\sigma}+s}{\widehat{\gamma}} \\ -e^s \frac{\widehat{\gamma}}{2s} + e^{-s} \frac{\widehat{\gamma}}{2s} & e^s \frac{\widehat{\sigma}+s}{2s} + e^{-s} \frac{-\widehat{\sigma}+s}{2s} \end{bmatrix} \\ &= \begin{bmatrix} \cosh s - \widehat{\sigma} \frac{\sinh s}{s} & -\widehat{\gamma} \frac{\sinh s}{s} \\ -\widehat{\gamma} \frac{\sinh s}{s} & \cosh s + \widehat{\sigma} \frac{\sinh s}{s} \end{bmatrix}, \end{aligned}$$

from which follow

$$(A.10) \quad c = -\widehat{\gamma} \frac{\sinh(\sqrt{\widehat{\gamma}^2 + \widehat{\sigma}^2})}{\sqrt{\widehat{\gamma}^2 + \widehat{\sigma}^2}} \quad \text{and} \quad d = \cosh(\sqrt{\widehat{\gamma}^2 + \widehat{\sigma}^2}) + \widehat{\sigma} \frac{\sinh(\sqrt{\widehat{\gamma}^2 + \widehat{\sigma}^2})}{\sqrt{\widehat{\gamma}^2 + \widehat{\sigma}^2}}.$$

Assumption 3.3 clearly holds:  $\psi$  is positive and  $d > 1$  (since it is the sum of a hyperbolic cosine and a positive number), meaning  $0 < \varphi = d^{-1} < 1$ .



**A.4. Proof for Example 3.11.** We will need to prove that the right-hand side of (3.17) is smaller than 1 when  $\varphi =: \varphi_{\text{ex}}$  and  $\psi =: \psi_{\text{ex}}$  are given by (A.7), and  $\tilde{\varphi} =: \varphi_{\Delta T} = \varphi_{\Delta T}^{(1)}$  and  $\tilde{\psi} =: \psi_{\Delta T} = \psi_{\Delta T}^{(1)}$  are given by (A.5). We introduce some auxiliary variables to simplify working with the exact propagators:

$$s := \sqrt{\hat{\sigma}^2 + \hat{\gamma}^2}, \quad a := \cosh(s), \quad \text{and} \quad b := \frac{\sinh(s)}{s}$$

such that  $d = a + \hat{\sigma}b$  and  $|c| = -c = \hat{\gamma}b$ . Since  $\hat{\sigma} > 0$ , it is trivial to see that  $a, b, d > 1$ . Furthermore,  $a > b$ , as becomes clear from their respective Maclaurin series

$$(A.11) \quad \cosh(s) = 1 + \frac{s^2}{2!} + \frac{s^4}{4!} + \cdots \quad \text{and} \quad \frac{\sinh(s)}{s} = 1 + \frac{s^2}{3!} + \frac{s^4}{5!} + \cdots.$$

To prove the bound in Example 3.11, we write

$$\begin{aligned} & \rho^* \leq 1 \\ \Leftrightarrow & (\varphi_{\Delta T} - \varphi_{\text{ex}})^2 + (\psi_{\Delta T} - \psi_{\text{ex}})^2 \leq (1 - \varphi_{\Delta T})^2 + \psi_{\Delta T}^2 \\ \Leftrightarrow & 2\varphi_{\Delta T}\varphi_{\text{ex}} - \varphi_{\text{ex}}^2 + 2\psi_{\Delta T}\psi_{\text{ex}} - \psi_{\text{ex}}^2 + 1 - 2\varphi_{\Delta T} \geq 0 \\ \Leftrightarrow & 2\varphi_{\text{ex}} - (1 + \hat{\sigma})\varphi_{\text{ex}}^2 + 2\hat{\gamma}\psi_{\text{ex}} - (1 + \hat{\sigma})\psi_{\text{ex}}^2 + (1 + \hat{\sigma}) - 2 \geq 0 \\ \Leftrightarrow & 2d(1 + \hat{\gamma}|c|) - d^2(1 - \hat{\sigma}) - (1 + \hat{\sigma})(1 + |c|^2) \geq 0. \end{aligned}$$

This expression contains one term that is twice a positive quantity, and two that might be negative. It holds if a single instance of the first term plus either one of the others is positive. The first of these conditions is

$$(A.12) \quad \begin{aligned} & d(1 + \hat{\gamma}|c|) \geq d^2(1 - \hat{\sigma}) \Leftrightarrow 1 + \hat{\gamma}|c| \geq d(1 - \hat{\sigma}) \\ \Leftrightarrow & 1 + \hat{\gamma}^2 b \geq (a + \hat{\sigma}y)(1 - \hat{\sigma}) \\ \Leftarrow & 1 + \hat{\gamma}^2 b \geq a(1 - \hat{\sigma}^2). \\ \Leftrightarrow & 1 + \hat{\gamma}^2 b - a(1 - \hat{\sigma}^2) \geq 0, \end{aligned}$$

where the unidirectional implication holds since  $a > b$ . To show that (A.12)'s last inequality holds, consider its left-hand side's derivative with respect to  $\hat{\gamma}^2$ :

$$(A.13) \quad \begin{aligned} & \frac{d}{d\hat{\gamma}^2}(1 + \hat{\gamma}^2 b - a(1 - \hat{\sigma}^2)) \\ & = b + \hat{\gamma}^2 \frac{d}{d\hat{\gamma}^2} b - (1 - \hat{\sigma}^2) \frac{d}{d\hat{\gamma}^2} a = b + \hat{\gamma}^2 \left( \frac{\cosh s}{2s^2} - \frac{\sinh s}{2s^3} \right) - (1 - \hat{\sigma}^2) \frac{\sinh s}{2s} \\ & = \left(1 - \frac{1}{2} + \frac{\hat{\sigma}^2}{2} - \frac{\hat{\gamma}^2}{2s^2}\right)b + \frac{\hat{\gamma}^2}{2s^2}a = \frac{\hat{\sigma}^2 + \hat{\sigma}^2\hat{\gamma}^2 + \hat{\sigma}^4}{2s^2}b + \frac{\hat{\gamma}^2}{2s^2}a. \end{aligned}$$

This derivative is always positive. In other words, if (A.12)'s last inequality holds for  $\hat{\gamma} \rightarrow 0$ , it holds for all  $\hat{\gamma}$ . In this limit, (A.12) becomes

$$(A.14) \quad 1 \geq \cosh(\hat{\sigma})(1 - \hat{\sigma}^2),$$

which holds for any  $\hat{\sigma}$  (multiply the first Maclaurin series in (A.11) in  $\hat{\sigma}$  by  $1 - \hat{\sigma}^2$ ).

The second inequality from earlier takes less effort:

$$\begin{aligned} & d(1 + \hat{\gamma}|c|) \geq (1 + \hat{\sigma})(1 + |c|^2) \Leftrightarrow (a + \hat{\sigma}b)(1 + \hat{\gamma}^2 b) \geq (1 + \hat{\sigma})(1 + \hat{\gamma}^2 b^2) \Leftarrow \\ & b(1 + \hat{\sigma})(1 + \hat{\gamma}^2 b) \geq (1 + \hat{\sigma})(1 + \hat{\gamma}^2 b^2) \Leftrightarrow (1 + \hat{\sigma})(y + \hat{\gamma}^2 b^2) \geq (1 + \hat{\sigma})(1 + \hat{\gamma}^2 b^2), \end{aligned}$$

where, again,  $a > b$  justifies the unidirectional implication. Since  $b > 1$ , this inequality holds and, together with the previous inequality, the bound is now proven.

**Acknowledgments.** The authors thank Ignace Bossuyt, Toon Ingelaere, and Vince Maes for their reviews and helpful comments, and Carlos Fonseca for pointing to [15] as the original reference to use in Lemma 5.3’s proof. This project received funding from the European High-Performance Computing Joint Undertaking (JU) under grant agreement No. 955701. The JU receives support from the EU’s Horizon 2020 programme. Karl Meerbergen’s work is supported by the Research Foundation Flanders grants G0B7818N and G088622N, and by the KU Leuven Research Council.

## REFERENCES

- [1] D. A. BINI, G. LATOUCHE, AND B. MEINI, *Numerical Methods for Structured Markov Chains*, Numer. Math. Sci. Comput., Oxford University Press, 2005.
- [2] A. BOUILLON, G. SAMAEY, AND K. MEERBERGEN, *On generalized preconditioners for time-parallel parabolic optimal control*, arXiv:2302.06406 [cs, math], (2023).
- [3] M. EMMETT AND M. MINION, *Toward an efficient parallel in time method for partial differential equations*, Commun. Appl. Math. Comput. Sci., 7 (2012), pp. 105–132.
- [4] M. J. GANDER AND L. HALPERN, *Time Parallelization for Nonlinear Problems Based on Diagonalization*, in Domain Decomposition Methods in Science and Engineering XXIII, vol. 116, Springer International Publishing, 2017, pp. 163–170.
- [5] M. J. GANDER, F. KWOK, AND J. SALOMON, *PARAOPT: A Parareal Algorithm for Optimality Systems*, SIAM J. Sci. Comput., 42 (2020), pp. A2773–A2802.
- [6] M. J. GANDER, J. LIU, S.-L. WU, X. YUE, AND T. ZHOU, *ParaDiag: Parallel-in-time algorithms based on the diagonalization technique*, arXiv:2005.09158 [cs, math], (2021).
- [7] M. J. GANDER AND S.-L. WU, *Convergence analysis of a periodic-like waveform relaxation method for initial-value problems via the diagonalization technique*, Numer. Math., 143 (2019), pp. 489–527.
- [8] A. GODDARD AND A. WATHEN, *A note on parallel preconditioning for all-at-once evolutionary PDEs*, ETNA - Electronic Transactions on Numerical Analysis, 51 (2019), pp. 135–150.
- [9] S. GÖTSCHHEL AND M. L. MINION, *An Efficient Parallel-in-Time Method for Optimization with Parabolic PDEs*, SIAM J. Sci. Comput., 41 (2019), pp. C603–C626.
- [10] Y. HE AND J. LIU, *A Vanka-type multigrid solver for complex-shifted Laplacian systems from diagonalization-based parallel-in-time algorithms*, Appl. Math. Lett., 132 (2022), p. 108125.
- [11] M. HINZE, R. PINNAU, M. ULBRICH, AND S. ULBRICH, eds., *Optimization with PDE Constraints*, no. 23 in Mathematical Modelling: Theory and Applications, Springer, 2009.
- [12] J.-L. LIONS, Y. MADAY, AND G. TURINICI, *Résolution d’EDP par un schéma en temps «pararéel»*, C.R. Acad. Sci. Paris Sér. I Math., 332 (2001), pp. 661–668.
- [13] J. LIU AND Z. WANG, *A ROM-accelerated Parallel-in-Time Preconditioner for Solving All-at-Once Systems from Evolutionary PDEs*, 2020.
- [14] J. LIU AND S.-L. WU, *A fast block  $\alpha$ -circulant preconditioner for all-at-once system from wave equations*, SIAM J. Matrix Anal. Appl., (2020).
- [15] L. LOSONCZI, *Eigenvalues and eigenvectors of some tridiagonal matrices*, Acta Math. Hung., 60 (1992), pp. 309–322.
- [16] E. McDONALD, J. PESTANA, AND A. WATHEN, *Preconditioning and iterative solution of all-at-once systems for evolutionary partial differential equations*, SIAM J. Sci. Comput.
- [17] B. N. PARLETT, *The Symmetric Eigenvalue Problem*, Classics in Applied Mathematics, Society for Industrial and Applied Mathematics, 1998.
- [18] M. K. RIAHI, J. SALOMON, S. J. GLASER, AND D. SUGNY, *Fully efficient time-parallelized quantum optimal control algorithm*, Phys. Rev. A, 93 (2016).
- [19] Y. SAAD AND M. H. SCHULTZ, *GMRES: A generalized minimal residual algorithm for solving nonsymmetric linear systems*, SIAM J. Sci. Statist. Comput., 7 (1986), pp. 856–869.
- [20] V. SIMONCINI AND M. BENZI, *Spectral properties of the Hermitian and skew-Hermitian splitting preconditioner for saddle point problems*, SIAM J. Matrix Anal. Appl., 26 (2004).
- [21] C. S. SKENE, M. F. EGGL, AND P. J. SCHMID, *A parallel-in-time approach for accelerating direct-adjoint studies*, Journal of Computational Physics, 429 (2021).
- [22] S.-L. WU, *Toward Parallel Coarse Grid Correction for the Parareal Algorithm*, SIAM J. Sci. Comput., 40 (2018), pp. A1446–A1472.
- [23] S.-L. WU AND J. LIU, *A Parallel-In-Time Block-Circulant Preconditioner for Optimal Control of Wave Equations*, SIAM J. Sci. Comput., (2020).
- [24] S.-L. WU AND T. ZHOU, *Diagonalization-based Parallel-in-time algorithms for parabolic PDE-constrained optimization problems*, ESAIM Control Optim. Calc. Var., (2020).